NPS-57BP72011A

NAVAL POSTGRADUATE SCHOOL

Monterey, California

ANALYSIS OF A THREE INCH
GUN LAUNCHED FINNED MOTOR CASE

BY

Robert E. Ball
and
David Salinas

January 1972

NAVAL POSTGRADUATE SCHOOL
Monterey, California

Rear Admiral A. S. Goodfellow, Jr., USN
Superintendent

Milton U. Clauser
Provost

ABSTRACT:

An analysis of a 3-inch gun launched finned motor case is performed in an attempt to determine the cause of failure. Two specific features of the problem are identified as the probable reasons for the buckling failure of the motor case.

TABLE OF CONTENTS

INTRODUCTION

The Naval Weapons Center, at China Lake, California, is presently in the process of developing a series of gun launched guided projectiles. Recent experimental firings of a 3-inch projectile showed the structural design of the motor case to be inadequate since the case buckled severely as the projectile passed through the gun barrel. The authors were asked to perform an analysis of the motor case to determine the cause of failure. In addition, the authors were asked to recommend a structural design of a 5 inch projectile that minimizes the motor case weight and to propose a design technique which can be used by engineers as a design tool in future gun launched guided projectile projects. This report concentrates on the analysis of the 3-inch motor case and the design technique.

The following four pages show 1) a drawing of the projectile; 2) and 3) high speed photographs of two firings; and 4) a picture of a buckled projectile in flight.

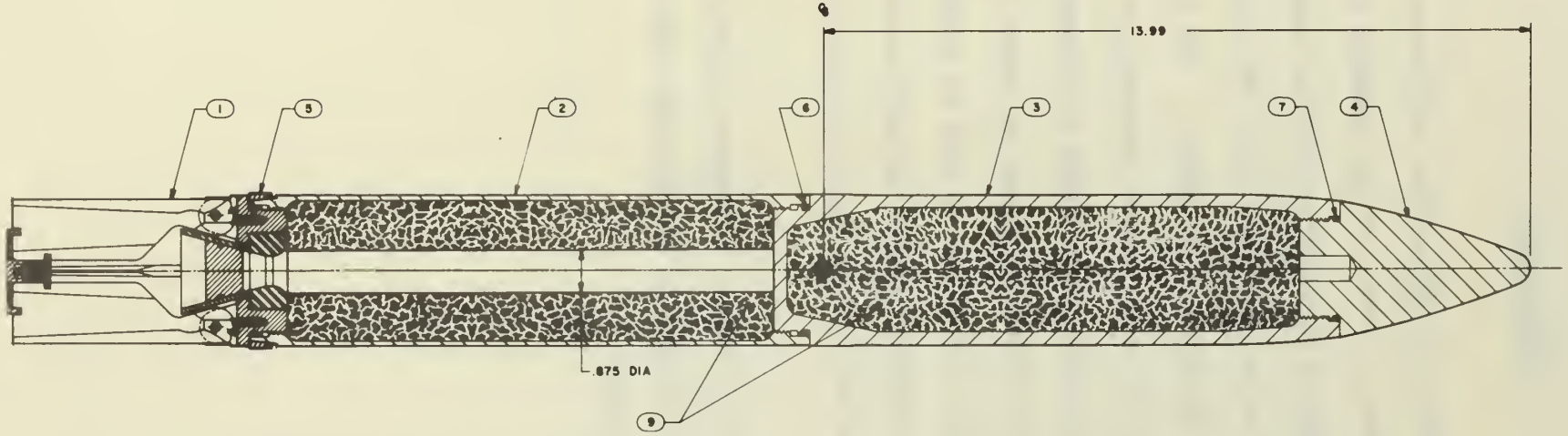

ITEM NO.	QTY REQD	CODE IDENT	PART NO. OR IDENTIFYING NO.	NOMENCLATURE OR DESCRIPTION	SPECIFICATION	NOTE	ZONE
9	AR			FMJBR			
8	AR			LOCTITE			
7	1		MS38173-134	PACKING, PREFORMED			
6	1		MS38173-141	PACKING, PREFORMED			
5	1		SK [illegible]	RING, OBTURATOR			
4	1		SK [illegible]	NOSE PLUG			
3	1		SK [illegible]	MOTOR CASE			
2	1		SK [illegible]	WARHEAD BODY, INERT			
1	1		SK [illegible]	NOZZLE FIN ASSEMBLY			

PARTS LIST

SK4500304

GENOA INDUSTRIES INC.
JEH 5-25-71

4573

PROJECTILE,
3 INCH 10 CALIBER
DUMMY

D 12934 SK4500304

SCALE 1/1 WEIGHT 10.8 LBS SHEET

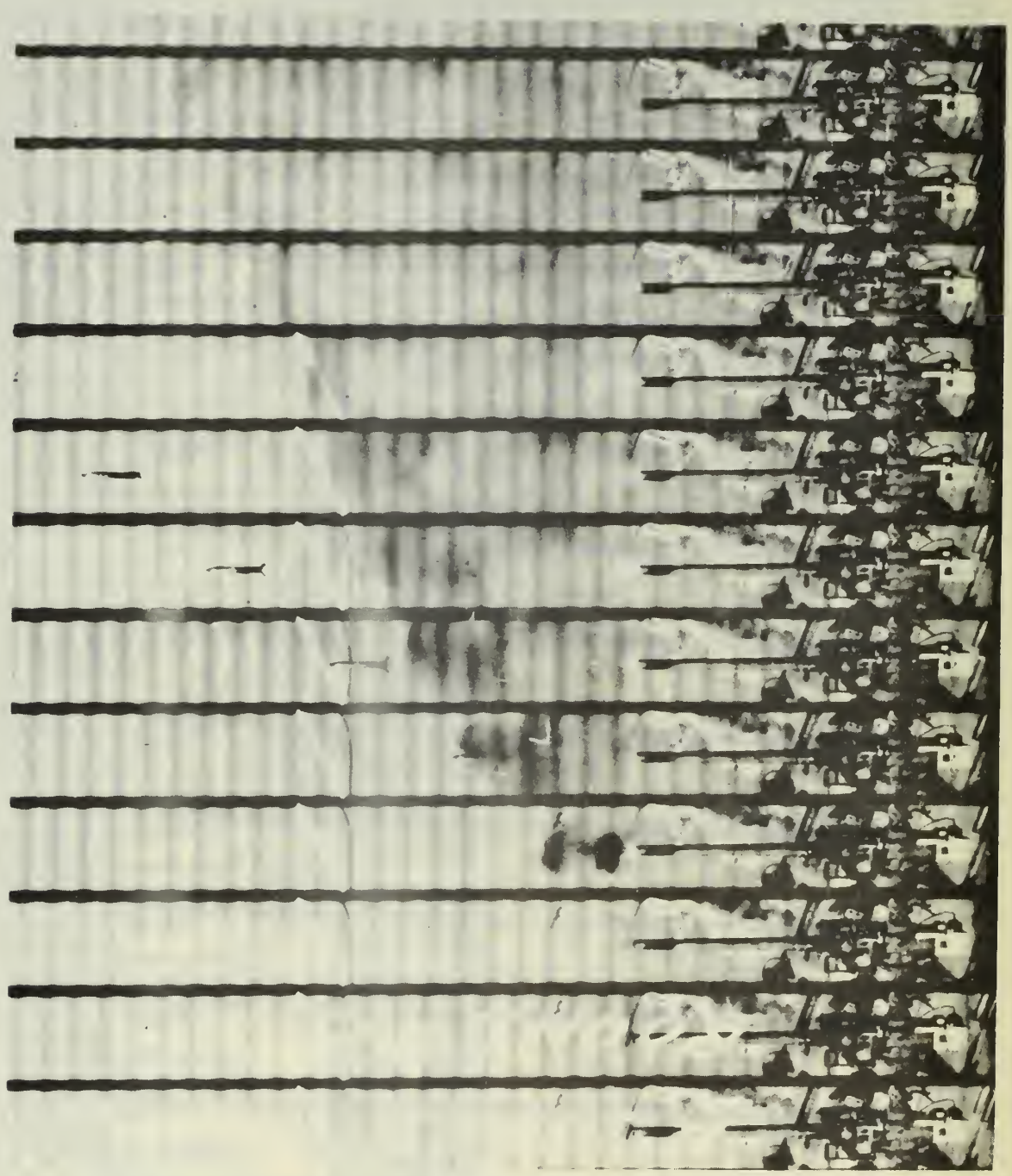

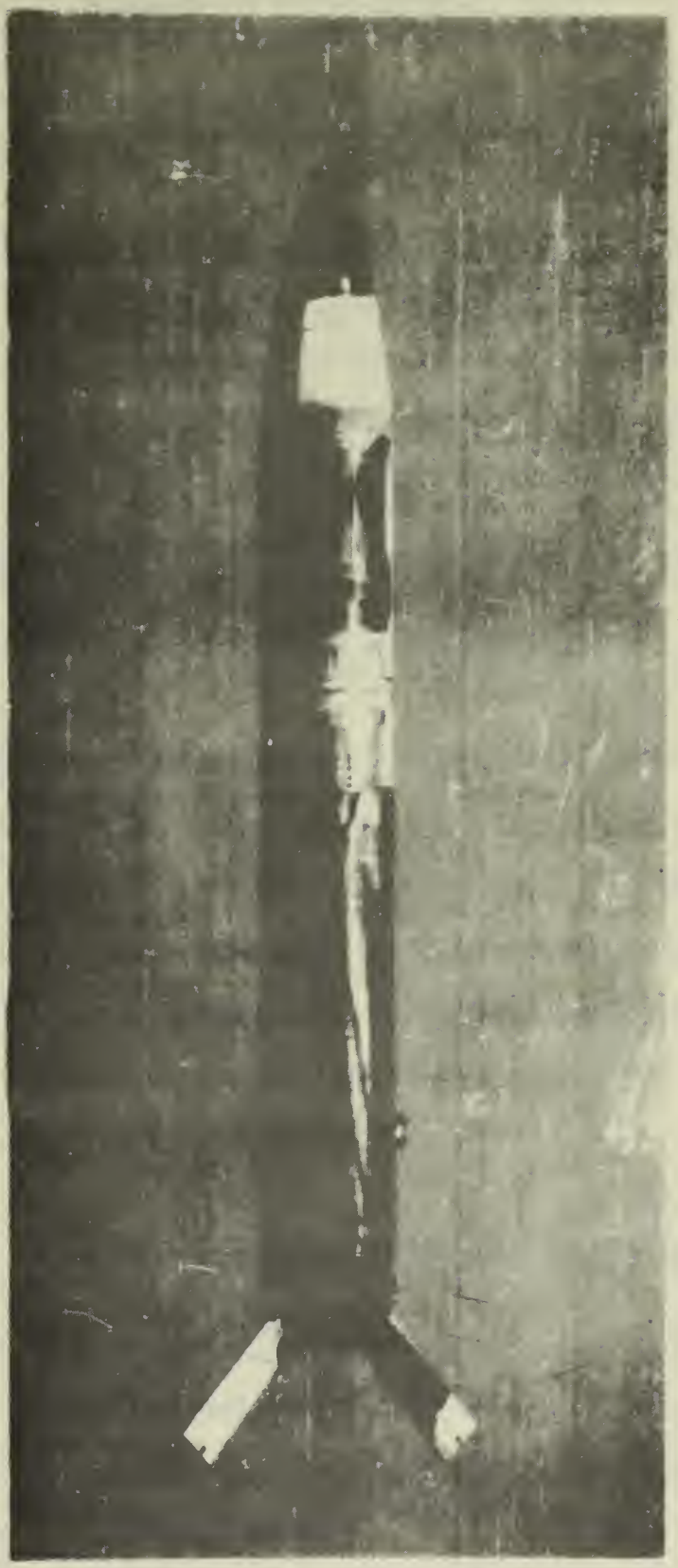

DESCRIPTION OF THE THREE-INCH PROJECTILE

The casing is 4130 steel alloy heat treated to 200,000 psi. From MIL-HDBK-5A, Feb 8, 1966:

Elastic modulus in tension and compression, $E = 29 \times 10^6$ psi

Modulus of rigidity, $G = 11 \times 10^6$ psi

Therefore

Poisson's ratio, $\nu = .32$

Density, $\omega = 0.283$ #/in^3

0.002 Compressive yield stress, $\sigma_{cy} = 198{,}000$ psi

Total projectile weight:

Warhead with filler	9.74 lbs	forward = 11.43 lbs
Fuse	1.69 lbs	
Motor case	1.99 lbs	motor = 5.58 lbs
Propellant	3.59 lbs	
Forward bulkhead	0.40 lbs	aft = 2.79 lbs
Nozzle plate	1.89 lbs	
Fins	0.31 lbs	
Fin Release	0.10 lbs	
Obturator	0.03 lbs	
Nozzle plug	0.06 lbs	
	19.80 lbs	

Length, L = 9.5 in

Radius, r = 1.5 in

Thickness, h = 0.08 in

DESCRIPTION OF THE EXTERNAL LOAD

The external load on the projectile consists of two parts; 1) the breech pressure at the base of the projectile, and 2) a lateral pressure on the sides of the case due to the breech pressure seeping beyond the obturator. A typical plot of the predicted barrel pressure as a function of time is shown in Fig. 1. According to NWC (Data sheet for 5 inch projectile, L. R., 10-20-71) the base pressure on the projectile is 0.9424 x breech pressure. Thus, a_{max}, the predicted maximum rigid body acceleration of the projectile, is

$$a_{max} = \frac{\text{maximum force}}{\text{total mass}} = \frac{(26.5 \text{ ksi})(0.9424)(\pi)(1.5 \text{ in.})^2}{19.8 \text{ lbs/g}} = 8{,}900 \text{ g}$$

where g is the acceleration due to gravity.

The lateral pressure in the motor case occurs when the obturator cracks. Photographs of the firings show smoke coming from the gun barrel before the projectile emerges, thus establishing the existence of this pressure. No estimates of the magnitude of this pressure are available. Future NWC obturator designs will attempt to eliminate this pressure.

DETERMINATION OF THE INTERNAL AXIAL FORCE

In order to obtain an estimate of the transient internal axial force in the motor case, the projectile subjected to the transient base pressure shown in Figure 1 is idealized as a one dimensional steel structure with a force $P_o \sin \frac{\pi t}{.012}$, $0 \leq t \leq .012$, at the aft end. The forward end of the projectile is taken as either free or fixed, these two conditions

being the extreme possibilities. The belief was that this analysis would provide a bounded estimate of the transient axial force. The details of the analysis and the results are presented in Appendix A. The essential result of the analysis is that the rise time of the pressure is very slow in relation to the wave speed of the case, and hence the internal axial force at any location along the case at any time is equal to the mass forward of that location multiplied by the rigid body acceleration of the projectile at that time. Thus, there is neither an amplification nor a reduction in the internal axial force due to dynamic effects.

Since the axial force in the case is dependent upon the distribution of the mass of the projectile, the question of the load path of the motor propellant becomes important. The propellant body force could either be transferred to a longitudinal shear load on the case or a compression load on the forward bulkhead of the aft end, depending to some extent upon the bonding condition between the propellant and the case. Since there was considerable uncertainty as to which path was the correct one, a two dimensional stress analysis was performed on the propellant for both the condition of bonding and of no bonding. The Rohm and Hass computer program AMG032A for the stress analysis of linear elastic, isotropic, axisymmetrically loaded, axisymmetric propellant gain with (or without) an orthotropic elastic motor case was used (Ref. 1). The details and results are presented in Appendix B. The essential conclusion drawn from the results for the bonded propellant is that the maximum shear stress on the case (and in the bond) is approximately 300 psi and approximately 80% of the total

Fig. 1 Predicted Barrel Pressure vs. Time

propellant body force is carried by longitudinal shear loading on the case and 20% by compression on the bulkhead at the aft end of the case. Of course, the unbonded propellant body force is carried entirely by a compression on the bulkhead.

Taking the results of these analyses into consideration, the forces at the forward and aft ends of the motor case are

$$P_{forward} = \left(\frac{11.43 \text{ lbs}}{g}\right)(8{,}900 \text{ g}) = 102 \text{ kips}$$

$$P_{aft} = 102 \text{ kips} + \left(\frac{1.99 + .8 \times 3.59 \text{ lbs}}{g}\right)(8{,}900 \text{ g})$$

$$= 145 \text{ kips}$$

for the bonded propellant (80% carried by the case) and

$$P_{aft} = 102 \text{ kips} + \left(\frac{1.99}{g}\right)(8{,}900 \text{ g}) = 120 \text{ kips}$$

for the unbonded propellant. The maximum stress due to these loads is

$$\sigma_{max} = (145 \text{ kips})/[(2\pi)(1.5 \text{ in.})(0.08 \text{ in.})]$$

$$= 192 \text{ ksi}$$

which is just below σ_{cy}.

DETERMINATION OF THE DYNAMIC RESPONSE OF THE CASE TO THE TRANSIENT AXIAL FORCE

Because the axial force is on the case for only a short period of time, the possibility exists that the case may not suffer large deformations for loads that are larger than the critical load for static buckling, i.e., the loading may be impulsive. This possibility is

investigated in Appendix C, where the critical static buckling mode of the case is subjected to the force $P_o \sin \frac{\pi t}{.012}$ and the elastic transient response is computed. Two estimates of the natural frequency of the critical buckling mode are used, one without the propellant mass attached and one with the propellant mass attached. The essential result from this analysis is that if the maximum value of the applied force, P_o, is equal to the critical load for static buckling the maximum magnitude of the buckled deflection is approximately 100-200 times larger than the initial imperfection in the shape of the critical buckling mode. For the manufacturing tolerances in this program this is a large deflection and represents a severe buckling condition. Thus, the loading is not impulsive and the maximum axial force must be less than the static buckling load to prevent severe buckling.*

DETERMINATION OF THE STATIC BUCKLING LOADS OF THE CASE

The results of the preceding analyses indicate that the motor case can be designed using standard procedures for estimating the static buckling strength of shells. Consequently, the following static loading conditions were considered:

(1a) Uniform axial compression, only, $P = P_{forward} = P_{aft}$

(1b) Linearly varying axial compression only, $P = P_{forward} + \pi(3 \text{ in})(x)q_s$

---

*A value of P_o equal to 90% of the critical load for static buckling causes an amplification of approximately 10 which may also represent severe buckling. This depends upon the magnitude of the imperfection that exists in the buckling mode shape prior to firing.

(2) Uniform external radial pressure only, q_r

(3) Combined uniform axial compression and uniform radial pressure, $P = P_{forward} = P_{aft}$, q_r

where q_r and q_s are the radial and longitudinal uniform external pressure components respectively, and x is the longitudinal coordinate (x=0 at the forward end).

The elastic buckling load for loading condition (1a) was determined using the formula presented in Ref. 2, page 528, and the computer program for the geometrically nonlinear analysis of arbitrarily loaded shells of revolution developed by Ball (Ref. 3). The results are shown in Fig. 2, where σ_{cr} is the critical axial buckling stress. The maximum predicted axial stress in the case due to the firing is 192 ksi and is also indicated in Fig. 2. Since σ_{cr} is much larger than σ_{cy}, the buckling is inelastic and the predicted elastic buckling loads are invalid. The inelastic buckling load for loading condition (1a) was estimated using the charts from Ref. 2, page 704, and is also given in Fig. 2.* Note that this stress is less than the maximum predicted axial stress in the shell. As a consequence of this, the case will buckle inelastically due to the axial load alone.

The elastic buckling load for loading condition (1b) was determined using the computer program of Ref. 3, and is shown in Fig. 2. For this condition all the propellant was assumed to be carried by a uniformly distributed shear stress on the motor case. The ratio of

---

*The result shown in Fig. 2 is a conservative estimate since NWC experimental results for the static buckling of a 0.065 in. thick cylinder indicated a higher buckling stress.

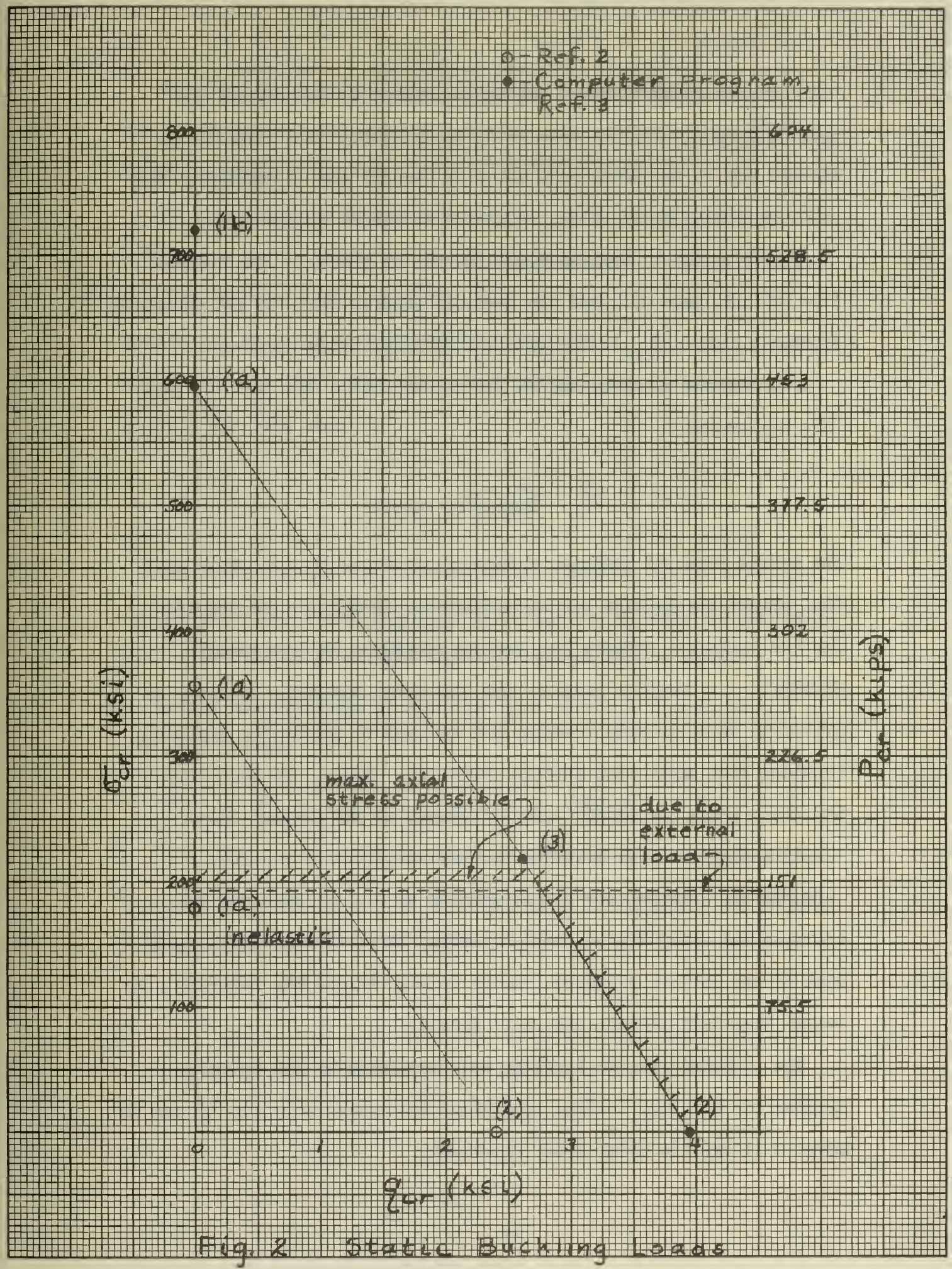

Fig. 2 Static Buckling Loads

axial stress at the forward end to the stress at the aft end was $\frac{11.43}{11.43 + 5.58} = .674$, the same ratio as the total mass ahead of the forward end to the total mass ahead of the aft end of the case. The critical stress shown in Fig. 2 is the stress at the aft end.

Buckling due to loading condition (2) is elastic. The results from Ref. 2, page 540, and the computer program (Ref. 3) are presented in Fig. 2, where q_{cr} is the critical external radial pressure.

For elastic buckling due to loading condition (3), Ref. 2, page 544, recommends

$$\frac{P}{P_{cr}} + \frac{q}{q_{cr}} = 1$$

The result from the computer program is given in Fig. 2. Note that this result agrees with the recommendation of Ref. 2. No results for the inelastic effects for loading condition (3) are readily available. A computer program that can treat inelastic buckling of cylinders under general loading must be used to obtain the inelastic buckling load under that loading condition. Hence, the stability of the shell along the dashed line is unknown at the present time.

Also shown in Fig. 2 is the maximum axial stress possible i.e. 200,000 ksi. Hence, the cross-hatching in Fig. 2 indicates the limiting values of the allowable loading. From this it can be seen that if the lateral pressure, due to leakage beyond the obturator, is larger than 2800 psi the case will buckle.

The critical elastic buckling mode predicted by the computer program for all four loading conditions was essentially $\sin \frac{\pi x}{L} \cos 2\theta$ where θ is the circumferential coordinate.

The details of the analyses using the formulas and charts in Ref. 2 are given in Appendix D. The computer results have been given to NWC personnel, Code 4573.

An examination of Fig. 2 reveals that there are significant differences in the predicted elastic buckling load obtained from Ref. 2 and from the computer program for loading conditions (1a) and (2). Apparently, there is need for further study here. The shell considered here is not exactly a thin shell, and the formulas in Ref. 2 may not be valid for this shell.

DESIGN TECHNIQUE

The following plan is recommended as a general design technique:

1. Determine the loads $P_{forward}$, P_{aft}, q_r, and q_s from the estimated weights and acceleration data and a propellant stress analysis.

2. Select the thickness of the case such that the maximum stress is less than 198 ksi.

3. Check to see if P_{aft} and q_s need to be changed.

4. Determine if the shell is stable (inelasticially) under the loads $P_{forward}$, P_{aft}, q_r, q_s. Note that q_r should include both the effect of the slumping propellant and the effect of the external pressure.

CONCLUSIONS

Several analyses have been performed on the 3-inch motor case to determine the cause of the buckling failure. The results of these analyses are:

1. The dynamic effects are insignificant and the case responds to the breech pressure as if the pressure were applied in a static sense, i.e. the maximum internal axial load in the case can be computed on the basis of the mass distribution and the maximum rigid body acceleration of the projectile.
2. The loading is not impulsive, i.e. it is on the case for a sufficient length of time such that the shell will collapse if the applied load equals the static buckling load of the case.
3. Approximately 80% of the propellant inertial load is carried by shear along the case when the propellant is bonded.
4. The case will buckle inelastically due to the axial load caused by the launch.
5. If the obturator cracks, 10-20% of the breech pressure acting as a lateral pressure is sufficient by itself to cause elastic buckling.
6. The predicted buckling mode for axial load and for lateral pressure is the same and is essentially identical to the observed buckled shape of the launched projectile.
7. The static buckling loads computed using the formulas in Ref. 2 are considerably lower than those predicted by the computer program of Ref. 3.

REFERENCES

1. Becker, Eric B. and Brisbane, John J., "Application of the Finite Element Method to Stress Analysis of Solid Propellant Rocket Grains, Vol. I and II," Rohm and Hass Company, Redstone Arsenal Research Division, Huntsville, Alabama, Report No. 5-76, Nov. 1965 and Jan. 1966.

2. Baker, E. H., et al., "Shell Analysis Manual," NASA Contractor Report CR-912, April 1968.

3. Ball, R. E., "A Geometrically Nonlinear Analysis of Arbitrarily Loaded Shells of Revolution," NASA Contractor Report NASA CR-909, Jan. 1968.

APPENDIX A

Transient Axial Response

Statement of the Problem

In this section, the case is idealized as a one dimensional, one material bar with an input force function $P(t) = P_o \sin \frac{\pi t}{\alpha}$, where α is the duration of the force and P_o the maximum intensity at $t = \pi/2$. The time length of the input force was taken as .012 sec. The boundary condition at the aft end of the bar (x=0) was taken as free, that is the axial force in the bar is equal to the forcing function. Two boundary conditions were considered at the forward end of the bar ($x=\ell$);

i) a free end with axial force equal to zero, and

ii) a fixed end with displacement equal to zero.

The actual boundary condition at the forward end is somewhere between these two idealized conditions. Hence the actual solution lies between the bounds obtained from the free-free and free-fixed problems.

The physical parameters taken in this problem, were the length of the bar ℓ = 10 in., and the Young's modulus for a steel bar $E = 30 \times 10^6$ lbs/in.^{2}.

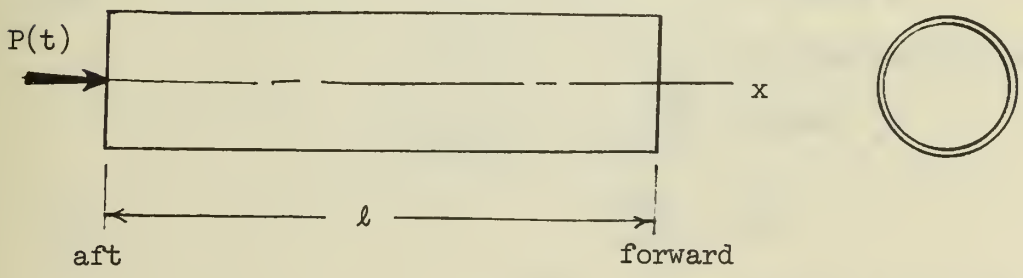

Governing equation for axial response

$$\frac{\partial^2 u}{\partial t^2} - c^2 \frac{\partial^2 u}{\partial x^2} = \begin{cases} \frac{-P(t)}{\rho \ell A} & \text{for moving bar} \\ 0 & \text{for stationary bar} \end{cases} \tag{1}$$

where u = displacement along x axis, x axis attached to the bar

t = time

c = speed of wave propagation $= \sqrt{\frac{E}{\rho}}$ (2)

E = Young's modulus of elasticity

ρ = mass density

ℓ = length

A = area

The initial conditions are

$$u\ (x,0) = 0 \tag{3}$$

$$u_t\ (x,0) = 0 \tag{4}$$

where u_t denotes velocity $\frac{\partial u}{\partial t}$.

The boundary conditions are

i) for free-free boundaries

$$u_x\ (0,t) = G(t) \tag{5}$$

$$u_x\ (\ell,t) = 0 \tag{6}$$

ii) for free-fixed boundaries

$$u_x\ (0,t) = G(t) \tag{7}$$

$$u\ (\ell,t) = 0 \tag{8}$$

In equations (5) through (9)

u_x denotes $\frac{\partial u}{\partial x}$

$$G(t) = \frac{P(t)}{EA} \tag{9}$$

where A is the area of the bar.

I. Axial response with free-free boundary conditions with

$$P(t) = P_o \sin \frac{\pi t}{\alpha} \tag{10}$$

Then

$$G(t) = \frac{P_o}{EA} \sin \frac{\pi t}{\alpha} = \bar{P} \sin \frac{\pi t}{\alpha} \tag{11}$$

We seek solution of equation (1), with initial conditions (3) and (4), and boundary conditions (5) and (6), with forcing function given by (10).

Solution by superposition. Consider solution u(x,t) in the form

$$u(x,t) = v(x,t) + U(x,t) \tag{12}$$

Then (1) becomes

$$v_{tt} + U_{tt} - c^2 (v_{xx} + U_{xx}) = - \frac{P(t)}{\rho \ell A} = -c^2 \frac{\bar{P}}{\ell} \sin \frac{\pi t}{\alpha} \tag{13}$$

Letting

$$f(x,t) = - U_{tt} + c^2 U_{xx} - \frac{P(t)}{\rho \ell A} \tag{14}$$

equation (13) becomes

$$v_{tt} - c^2 v_{xx} = f(x,t) \tag{15}$$

Boundary conditions (5) and (6) become

$$v_x (0,t) = G(t) - U_x (0,t) \tag{16}$$

$$v_x (\ell,t) = -U_x (\ell,t) \tag{17}$$

and initial conditions (3) and (4) become

$$v (x,0) = -U (x,0) \tag{18}$$

$$v_t(x,0) = -U_t(x,0) \tag{19}$$

$U(x,t)$ is chosen so that equations (16) and (17) become homogeneous boundary conditions in v. Here we take

$$U(x,t) = (x - \frac{x^2}{2\ell})\, G(t) \tag{20}$$

With equation (20) we find

i) boundary conditions (16) and (17) become

$$v_x(0,t) = 0 \tag{21}$$

$$v_x(\ell,t) = 0 \tag{22}$$

ii) initial conditions (18) and (19) become,

$$v(x,0) = - U(x,0) = (x - \frac{x^2}{2})\, G(0)$$

But $G(0) = 0$, hence $v(x,0) = 0$

$$v_t(x,0) = - U_t(x,0) = (x - \frac{x^2}{2\ell})\, G_t(0) = \Psi(x)$$

Since $G_t(0) = \bar{P}\,\frac{\pi}{\alpha}\,\Psi(x) = \frac{\pi \bar{P}}{\alpha}(x - \frac{x^2}{2\ell})$

$$v(x,0) = 0 \tag{23}$$

$$v_t(x,0) = \Psi(x) \tag{24}$$

where

$$\Psi(x) = \frac{\pi \bar{P}}{\alpha}\,(x - \frac{x^2}{2\ell}) \tag{25}$$

The solution to the boundary value problem in $v(x,t)$ defined by equations (15), (21) - (24) is sought. A solution in the form of a Fourier series is assumed, say

$$v(x,t) = \sum_{n=0=}^{\infty} v_n\,(t) \cos \frac{n\pi x}{\ell} \tag{26}$$

which satisfies boundary conditions (21) and (22). Functions $f(x,t)$ and $\Psi(x)$ are also expanded into their Fourier series,

$$f(x,t) = \sum_{n=0}^{\infty} f_n(t) \cos \frac{n\pi x}{\ell} \tag{27}$$

where

$$f_o(t) = \frac{1}{\ell} \int_0^{\ell} f(\xi,t)\, d\xi \tag{28}$$

$$f_n(t) = \frac{2}{\ell} \int_0^{\ell} f(\xi,t) \cos \frac{n\pi\xi}{\ell}\, d\xi \qquad n > 0 \tag{29}$$

and

$$\Psi(x) = \sum_{n=0}^{\infty} \Psi_n \cos \frac{n\pi x}{\ell} \tag{30}$$

where

$$\Psi_o = \frac{1}{\ell} \int_0^{\ell} \Psi(\xi)\, d\xi \tag{31}$$

$$\Psi_n = \frac{2}{\ell} \int_0^{\ell} \Psi(\xi) \cos \frac{n\pi\xi}{\ell}\, d\xi \qquad n > 0 \tag{32}$$

Substituting expressions (26), (27) and (30) into equations (15), (23), and (24) yields

$$\sum_{n=0}^{\infty} \cos \frac{n\pi x}{\ell} \left\{ \frac{d^2 v_n(t)}{dt^2} + c^2 \left(\frac{n\pi}{\ell} \right)^2 v_n(t) - f_n(t) \right\} = 0 \tag{33}$$

$$\sum_{n=0}^{\infty} \cos \frac{n\pi x}{\ell}\, v_n(0) = 0 \tag{34}$$

$$\sum_{n=0}^{\infty} \cos \frac{n\pi x}{\ell} \left\{ \frac{d\, v_n(0)}{dt} - \Psi_n \right\} = 0 \tag{35}$$

Equations (33) - (35) are satisfied if for each n, (n=0,1,2,...)

$$\frac{d^2 v_n(t)}{dt^2} + c^2 \left(\frac{n\pi}{\ell}\right)^2 v_n(t) = f_n(t) \tag{36}$$

$$v_n(0) = 0 \tag{37}$$

$$\frac{dv_n(0)}{dt} = \Psi_n \tag{38}$$

Equations (36) - (38) may be numerically solved on the computer (using Runga-Kutta or some other scheme) for $v_n(t)$, for n=0,1,2,..., where the tilda denotes the numerical approximation solution. Hence for a convergent series,

$$v(x,t) = \sum_{n=0}^{\infty} v_n(t)\cos\frac{n\pi x}{\ell} \simeq \sum_{n=0}^{\infty} \tilde{v}_n(t)\cos\frac{n\pi x}{\ell} = \tilde{v}(x,t) \tag{39}$$

Once $\tilde{v}(x,t)$ is obtained, we return to equation (12) to find

$$u(x,t) = v(x,t) + U(x,t) \simeq \tilde{v}(x,t) + U(x,t) = \tilde{u}(x,t) \tag{40}$$

Hence,

$$u(x,t) \simeq \sum_{n=0}^{N} \tilde{v}_n(t) \cos\frac{n\pi x}{\ell} + U(x,t) \tag{41}$$

The force is given by

$$F = EA\frac{\partial u}{\partial x} = \left\{-\sum_{n=1}^{N} \frac{n\pi}{\ell} \tilde{v}_n(t) \sin\frac{n\pi x}{\ell} + \frac{\partial U}{\partial x}(x,t)\right\} EA \tag{42}$$

Note that F does not depend upon the n=0, or rigid body term.

Numerical solution of

$$\frac{d^2 v_n(t)}{dt^2} + c^2 \left(\frac{n\pi}{\ell}\right)^2 v_n(t) = f_n(t) \qquad n = 1,2,\ldots \tag{36}$$

$$v_n(0) = 0 \tag{37}$$

$$\frac{dv_n(0)}{dt} = \Psi_n \tag{38}$$

Recall eq. (29) for $n > 0$

$$f_n(t) = \frac{2}{\ell}\int_0^{\ell} f(\xi,t)\cos\frac{n\pi\xi}{\ell}\,d\xi = \frac{2}{\ell}\int_0^{\ell}\left[\left(-\xi + \frac{\xi^2}{2\ell}\right) G_{tt} - \frac{c^2 G}{\ell} - \frac{P(t)}{\rho\ell A}\right]\cos\frac{n\pi\xi}{\ell}\,d\xi$$

$$= \frac{2}{\ell}\left[G_{tt}\left\{-\frac{1}{\left(\frac{n\pi}{\ell}\right)^2}\cos\frac{n\pi\xi}{\ell} - \frac{1}{\left(\frac{n\pi}{\ell}\right)}\xi\sin\frac{n\pi\xi}{\ell} + \frac{2\xi}{2\ell\left(\frac{n\pi}{\ell}\right)^2}\cos\frac{n\pi\xi}{\ell}\right.\right.$$

$$\left. - \frac{2}{2\ell\left(\frac{n\pi}{\ell}\right)^3}\sin\frac{n\pi\xi}{\ell} + \frac{\xi^2}{2\ell\left(\frac{n\pi}{\ell}\right)}\sin\frac{n\pi\xi}{\ell}\right\}$$

$$\left. - \left(\frac{c^2}{\ell} G + \frac{P}{\rho\ell A}\right)\frac{\ell}{n\pi}\sin\frac{n\pi\xi}{\ell}\right]_0^{\ell}$$

Therefore

$$f_n(t) = \frac{2\ell}{n^2\pi^2} G_{tt} = -\frac{2\ell}{\alpha^2 n^2}\bar{P}\sin\frac{\pi t}{\alpha} \tag{44}$$

or $$f_n = K_n \sin\frac{\pi t}{\alpha} \tag{45}$$

where $$K_n = -\frac{2\ell\bar{P}}{n^2\alpha^2} \tag{46}$$

Let $\beta_n = \frac{v_n}{K_n}$, then eqs. (36) to (38) become,

$$\frac{d^2 \beta_n(t)}{dt^2} + c^2 \left(\frac{n\pi}{\ell}\right)^2 \beta_n = \sin \frac{\pi t}{\alpha} \tag{47}$$

$$\beta_n(0) = 0 \tag{48}$$

$$\frac{d\beta_n}{dt}(0) = \frac{\Psi_n}{K_n} \tag{49}$$

Recall equations (32) and (25),

$$\Psi_n = \frac{2}{\ell} \int_0^{\ell} \Psi(\xi) \cos \frac{n\pi\xi}{\ell} \, d\xi$$

$$\Psi_n = \frac{2}{\ell} \int_0^{\ell} \frac{\pi \bar{P}}{\alpha} \left(\xi - \frac{\xi^2}{2\ell}\right) \cos \frac{n\pi\xi}{\ell} = \frac{2\pi\bar{P}}{\alpha\ell} \left(\frac{-\ell^2}{n^2\pi^2}\right) \tag{50}$$

$$\frac{\Psi_n}{K_n} = + \frac{\alpha}{\pi} = + 3.82 \times 10^{-3} \tag{51}$$

for $\alpha = .012$ sec.

Hence we solve for $\beta_n(t)$ from the following equations

$$\frac{d^2\beta}{dt^2} + c^2 \left(\frac{n\pi}{\ell}\right)^2 \beta_n = \sin \frac{\pi t}{\alpha} \tag{52}$$

$$\beta_n(0) = 0 \tag{53}$$

$$\frac{d\beta_n(0)}{dt} = \frac{\alpha}{\pi} = 3.82 \times 10^{-3} \qquad \text{for } \alpha = .012 \tag{54}$$

After obtaining $\beta_n(t)$ from the computer we find

$$\tilde{v}_n(t) = K_n \beta_n = - \frac{2}{n^2 \alpha^2} \ell \bar{P} \beta_n(t) \tag{55}$$

Finally then the force per unit P is

$$\frac{F}{P} = \left\{ - \sum_{n-1}^{N} \frac{n\pi}{\ell} \frac{\tilde{v}_n(t)}{\bar{P}} \sin \frac{n\pi x}{\ell} + \frac{1}{\bar{P}} \frac{\partial U(x,t)}{\partial x} \right\} EA$$

Therefore

$$\frac{F}{P_o} = \sum_{n=1}^{N} \frac{2\pi}{\alpha^2 n} \beta_n(t) \sin \frac{n\pi x}{\ell} + \left(1 - \frac{x}{\ell}\right) \sin \frac{\pi t}{\alpha} \qquad (56)$$

The latter term is the internal force due to the rigid body acceleration. The terms under the summation sign introduce the transient dynamics due to the elasticity of the bar.

II. Axial response with free-fixed boundary conditions with

$$P(t) = P_o \sin \frac{\pi t}{.012} \qquad (10)$$

A solution of equation (1), with initial conditions (3) and (4), and boundary conditions (7) and (8), with forcing function (10) is sought.

The method proceeds as before, except here we take

$$U(x,t) = (x-\ell)\, G(t) \qquad (57)$$

Boundary conditions on v(x,t) become

$$v_x(0,t) = 0 \qquad (58)$$

$$v(\ell,t) = 0 \qquad (59)$$

The governing equation in v(x,t) is

$$v_{tt} - c^2 v_{xx} = f(x,t) \qquad (60)$$

where

$$f(x,t) = - U_{tt} + c^2 U_{xx} \tag{61}$$

$$= - (x-\ell)\, G_{tt}$$

The initial conditions are

$$v(x,0) = 0 \tag{62}$$

$$v_t(x,0) = (x-\ell)\, G_t(0) = \Psi(x) \tag{63}$$

where

$$\Psi(x) = \frac{\pi P}{\alpha} (x-\ell) \tag{64}$$

Assume the Fourier expansion

$$v(x,t) = \sum_{n=1,3,\ldots}^{\infty} v_n(t) \cos \frac{n\pi x}{2\ell} \tag{65}$$

which satisfies boundary conditions (58) and (59). As before $f(x,t)$ and $\Psi(x)$ are expanded into Fourier series,

$$f(x,t) = \sum_{n=1,3,\ldots}^{\infty} f_n(t) \cos \frac{n\pi x}{2\ell} \tag{66}$$

$$f_0(t) = \frac{1}{2\ell} \int_0^{2\ell} f(\xi,t)\, d\xi \tag{67}$$

$$f_n(t) = \frac{1}{\ell} \int_0^{2\ell} f(\xi,t) \cos \frac{n\pi\xi}{2\ell}\, d\xi \qquad n > 0 \tag{68}$$

$$\Psi(x) = \sum_{n=1,3,\ldots}^{\infty} \Psi_n \cos \frac{n\pi x}{2\ell} \tag{69}$$

$$\Psi_n = \frac{1}{\ell} \int_0^{2\ell} \Psi(\xi) \cos \frac{n\pi\xi}{2\ell}\, d\xi \qquad n > 0 \tag{70}$$

$$\Psi_o = \frac{1}{2\ell} \int_0^{2\ell} \Psi(\xi) \cos \frac{n\pi\xi}{2\ell}\, d\xi$$

Substituting eqs. (65) - (70) into eq. (60), (62) and (63) yields

$$\sum_{n=1,3,\ldots}^{\infty} \cos \frac{n\pi x}{2\ell} \left\{ \frac{d^2 v_n(t)}{dt^2} + c^2 \left(\frac{n\pi}{2\ell}\right)^2 v_n(t) - f_n(t) \right\} = 0 \tag{71}$$

$$\sum_{n=1,3,\ldots}^{\infty} \cos \frac{n\pi x}{2\ell} \; v_n(0) = 0 \tag{72}$$

$$\sum_{n=1,3,\ldots}^{\infty} \cos \frac{n\pi x}{2\ell} \left\{ \frac{dv_n(0)}{dt} - \Psi_n \right\} = 0 \tag{73}$$

Again we seek the solution to the equations

$$\frac{d^2 v_n}{dt^2} + c^2 \left(\frac{n\pi}{2\ell} \right)^2 v_n = f_n \tag{74}$$

$$v_n(0) = 0 \tag{75}$$

$$\frac{dv_n(0)}{dt} = \Psi_n \tag{76}$$

for n = 1,3,5,... Numerical solution for a finite number of n = 1,3,5,... N yields the approximate solution, $v_n(t)$, hence

$$\tilde{v}(x,t) = \sum_{n=1,3,\ldots}^{N} \tilde{v}_n(t) \cos \frac{n\pi x}{2\ell} \tag{77}$$

Then

$$u(x,t) \simeq \sum_{n=1,3,\ldots}^{N} \tilde{v}_n(t) \cos \frac{n\pi x}{2\ell} + (x-\ell)\, G(t) \tag{78}$$

Finally

$$\frac{\partial u(x,t)}{\partial x} \simeq - \sum_{n=1,3,\ldots}^{N} \frac{n\pi}{2\ell} \tilde{v}_n(t) \sin \frac{n\pi x}{2\ell} + G(t) \tag{79}$$

Numerical solution of

$$\frac{d^2 v_n}{dt^2} + c^2 \left(\frac{n\pi}{2\ell}\right)^2 v_n = f_n$$

$$v_n(0) = 0$$

$$\frac{dv_n(0)}{dt} = \Psi_n \qquad \text{for } n = 1,3,5,\ldots$$

Calculation of $f_n(t)$ and Ψ_n for $n > 0$

$$f_n(t) = \frac{1}{\ell} \int_0^{2\ell} f(\xi,t) \cos \frac{n\pi\xi}{2\ell}\, d\xi = \frac{1}{\ell} \int_0^{2\ell} (\ell-\xi)\, G_{tt} \cos \frac{n\pi\xi}{2\ell}\, d\xi \qquad (80)$$

$$\frac{1}{G_{tt}} f_n(t) = \begin{cases} 0 & \text{for } n = 2,4,6,.. \\ \dfrac{8\ell}{n^2 \pi^2} & \text{for } n = 1,3,5,.. \end{cases} \qquad (81)$$

$$\Psi_n = \frac{1}{\ell} \int_0^{\ell} \Psi(\xi) \cos \frac{n\pi\xi}{2\ell}\, d\xi = \frac{1}{\ell} \int_0^{\ell} \frac{\pi P}{.012} (\xi-\ell) \cos \frac{n\pi\xi}{2\ell}\, d\xi \qquad (82)$$

$$\Psi_n = \frac{\pi P}{.012} \begin{cases} 0 & \text{for n even} \\ \dfrac{-8\ell}{n^2 \pi^2} & \text{for n odd} \end{cases} \qquad (83)$$

Hence we seek the solution of

$$\frac{d^2 v_n(t)}{dt^2} + c^2 \left(\frac{n\pi}{2\ell}\right)^2 v_n = \frac{-8\ell P}{\alpha^2 n^2} \sin \frac{\pi t}{.012} \qquad (84)$$

$$v_n(0) = 0 \qquad \text{for } n=1,3,5,\ldots \qquad (85)$$

$$\frac{dv_n}{dt}(0) = \frac{-8\ell}{n^2 \pi^2} \quad \frac{\pi P}{\alpha} \qquad (86)$$

Let $K_n = \dfrac{-8\ell P}{\alpha^2 n^2}$, and define $\beta_n = v_n/K_n$, (87)

then the above equations become,

$$\frac{d^2\beta_n}{dt^2} + c^2 \left(\frac{n\pi}{2\ell}\right)^2 \beta_n = \sin \frac{\pi t}{\alpha} \tag{88}$$

$$\beta_n(0) = 0 \qquad n = 1,3,5,\ldots \tag{89}$$

$$\frac{d\beta_n}{dt}(0) = \frac{\alpha}{\pi} = + 3.82 \times 10^{-3} \quad \text{for } \alpha = .012 \text{ sec} \tag{90}$$

After β_n is determined, we have

$$v_n(t) = K_n \beta_n = \frac{-8\ \ell\ P}{(.012)^2\ n^2}\ \beta_n(t) \qquad n=1,3,5\ldots \tag{91}$$

and

$$\frac{F}{P_0} = \sum_{n=1,3,\ldots}^{N} \frac{4\pi}{\alpha^2\ n} \beta_n(t) \sin \frac{n\pi x}{2\ell} + \sin \frac{\pi t}{\alpha} \tag{92}$$

for the solution of a free-fixed bar. The latter term represents the static response to the end force. The terms under the summation sign introduce the dynamic effects.

III. Results

The time history F/P_o at x/ℓ = 0,0.25,0.5,0.75 and 1 are given in Figs. A1-A5 for the free-free bar with α = .012 sec. Figs. A6-A10 show the corresponding values of F/P_o for the free-fixed bar. Figure A11 shows the history of F/P_o at x/ℓ = 0.5 for α = 0.0012 and Fig. A12 shows the history at x/ℓ = 0.5 for α = 0.012 and F = 3×10^6 psi for the free-free bar. These figures are from a plotter. The solution

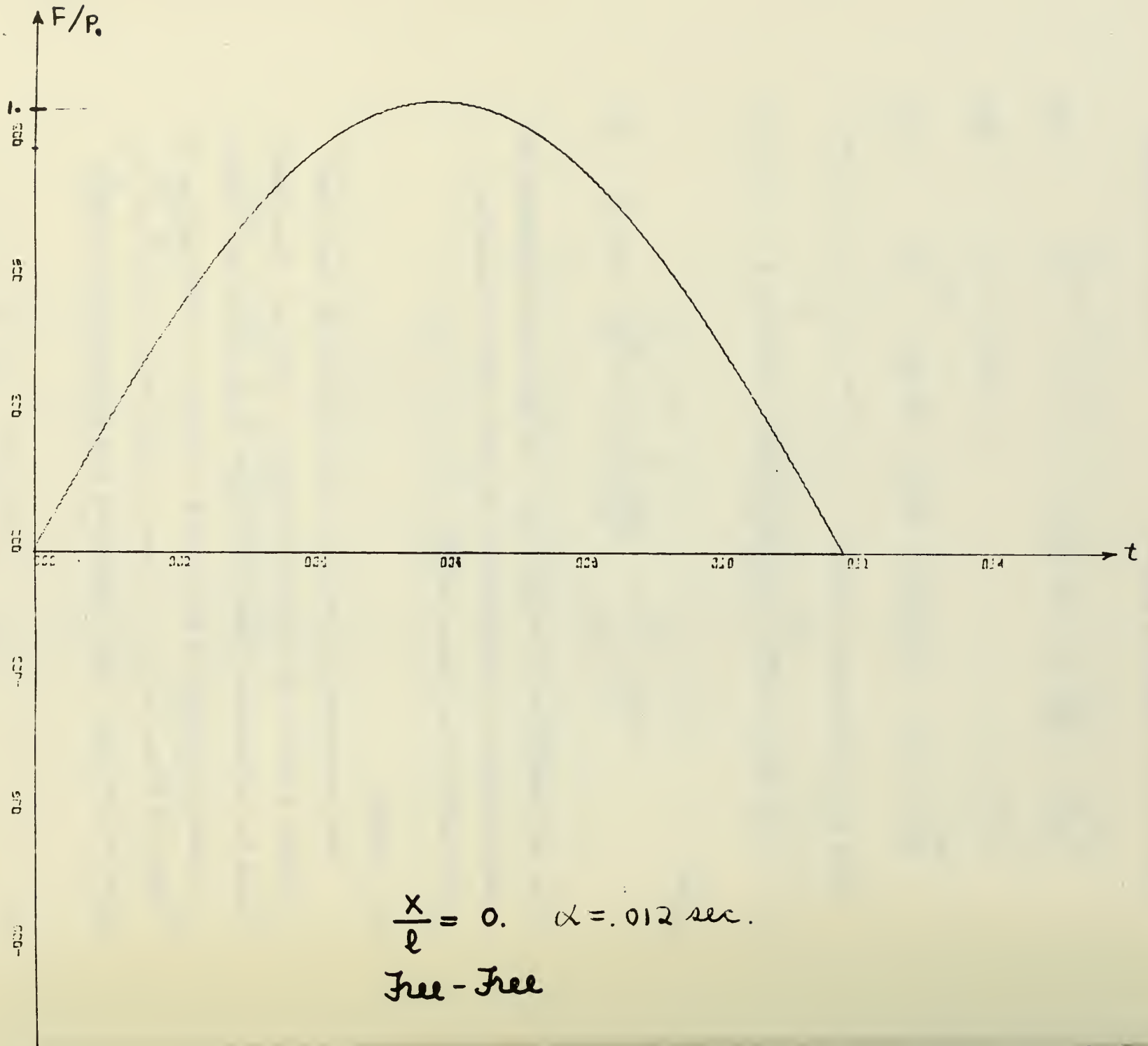

$\frac{x}{\ell} = 0.$ $\alpha = .012$ sec.

Free - Free

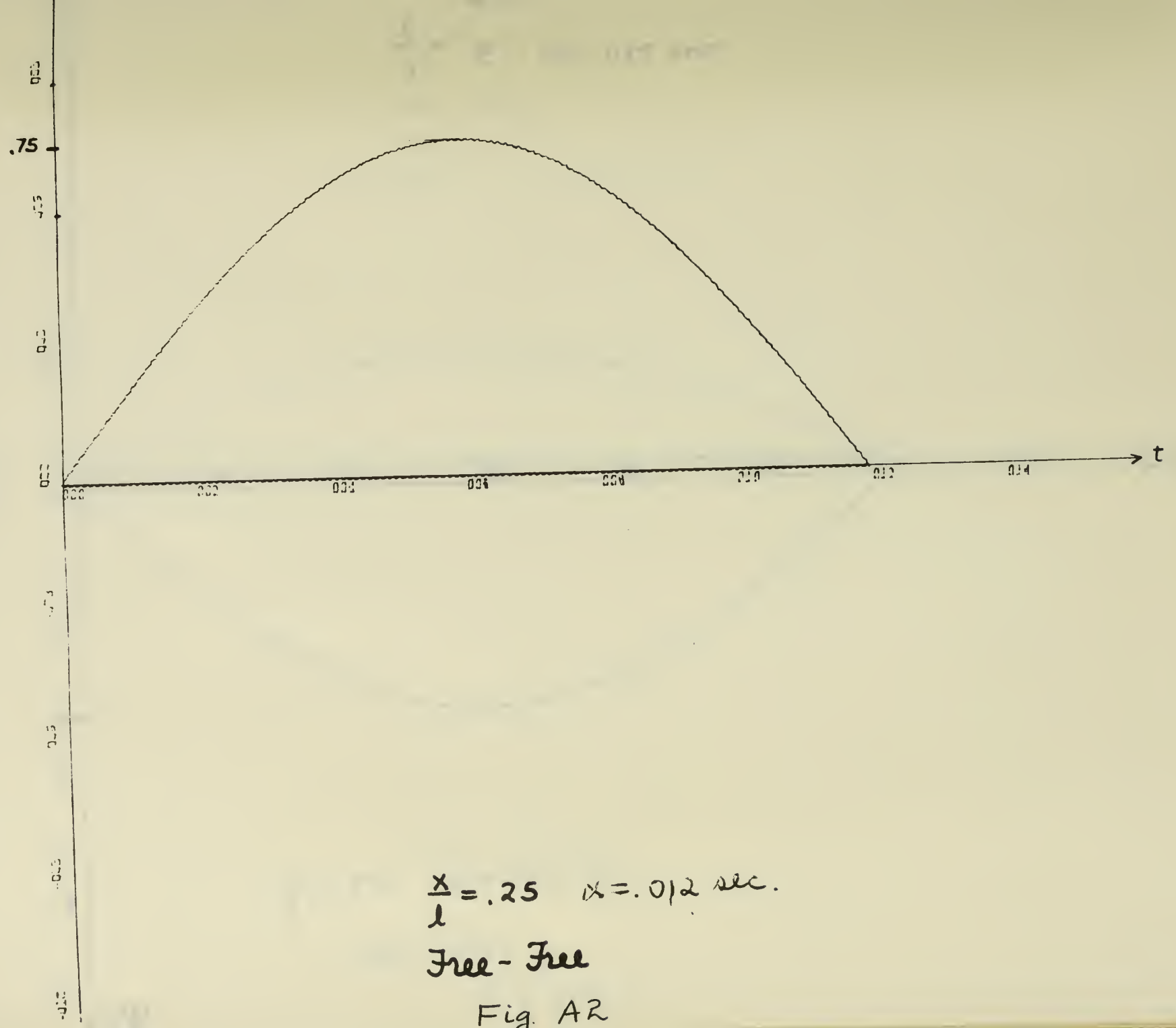

$\frac{x}{l} = .25 \quad x = .012$ sec.

Free - Free

Fig. A2

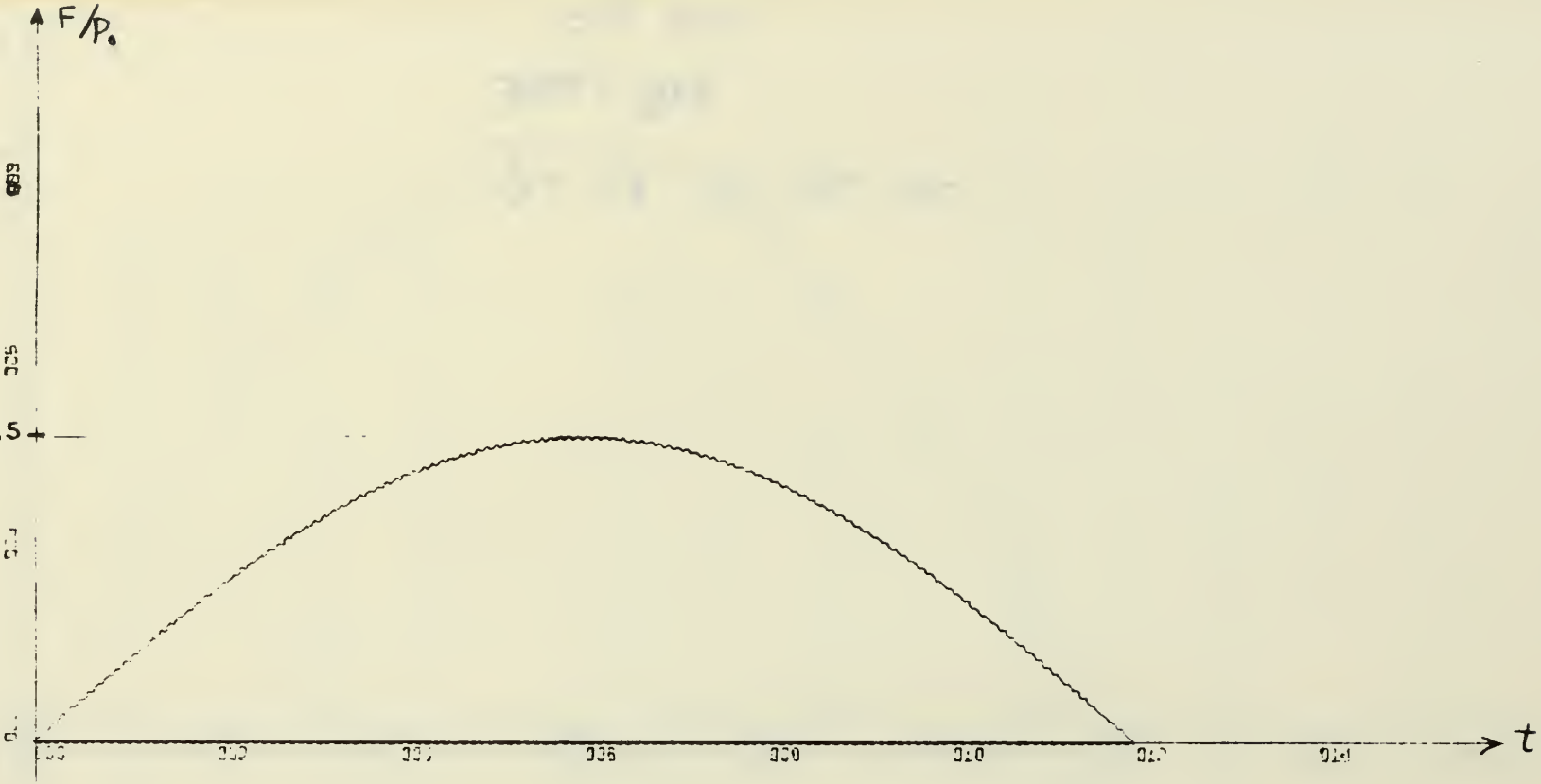

$\frac{x}{\ell} = .5 \quad \alpha = .012$ sec.

Free - Free

$\frac{x}{\ell} = .75$ $\alpha = .012$ sec

free - free

Fig. A4

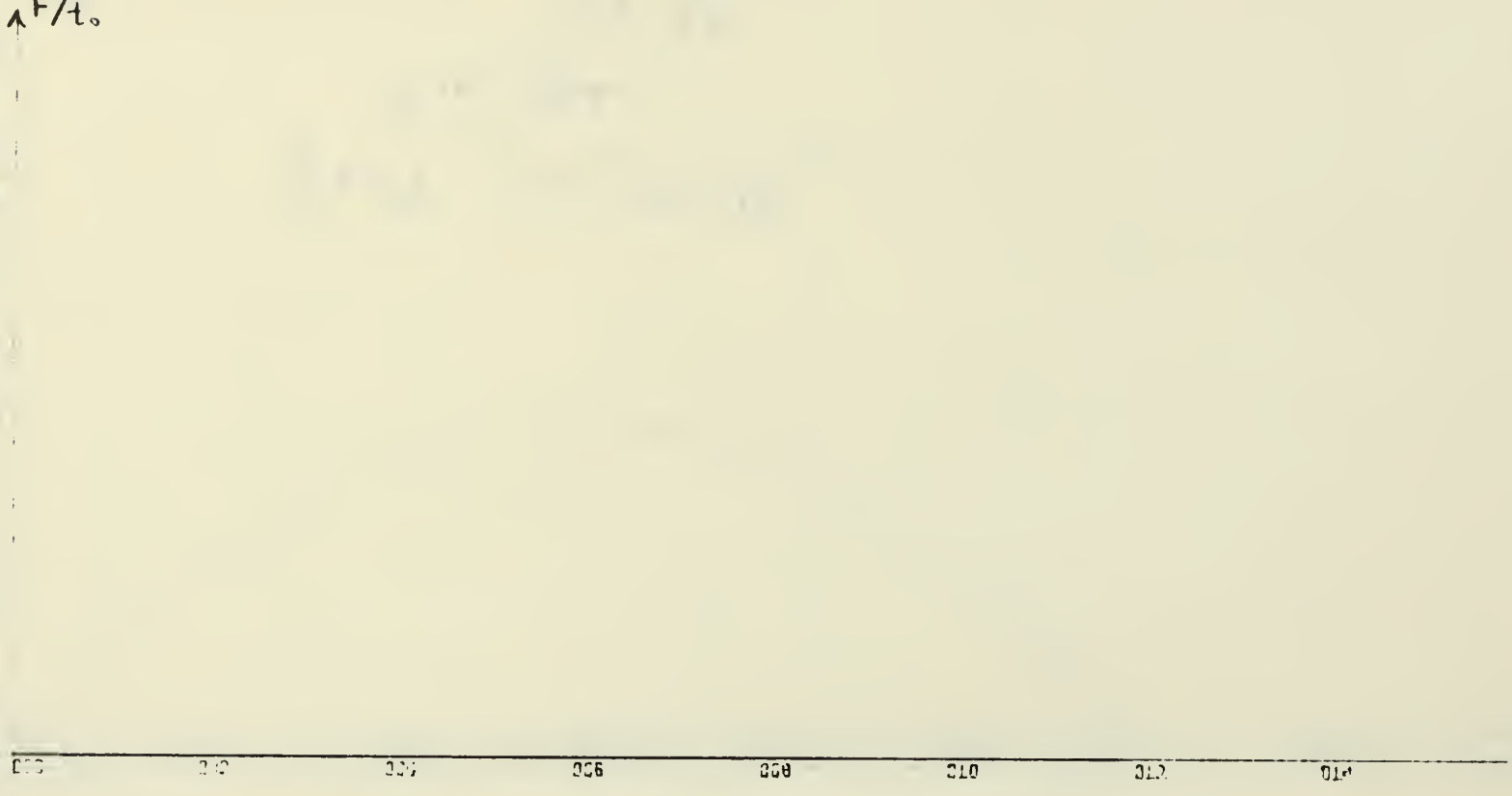

$\frac{x}{\ell} = 1.$ $\alpha = .012$ sec.

Free - Free

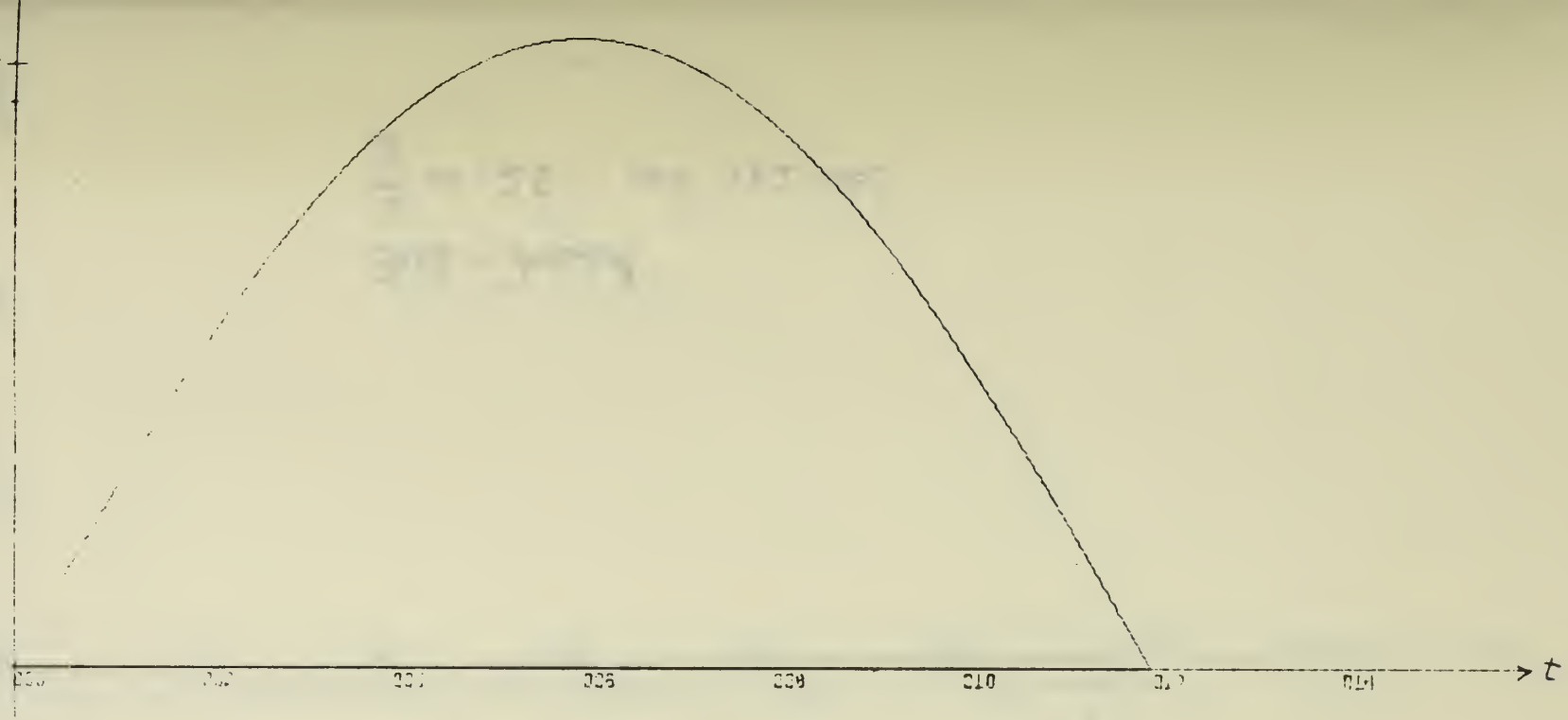

Free - Fixed

$\frac{x}{\ell} = 0.$ $\alpha = .012$ sec.

Fig. A6

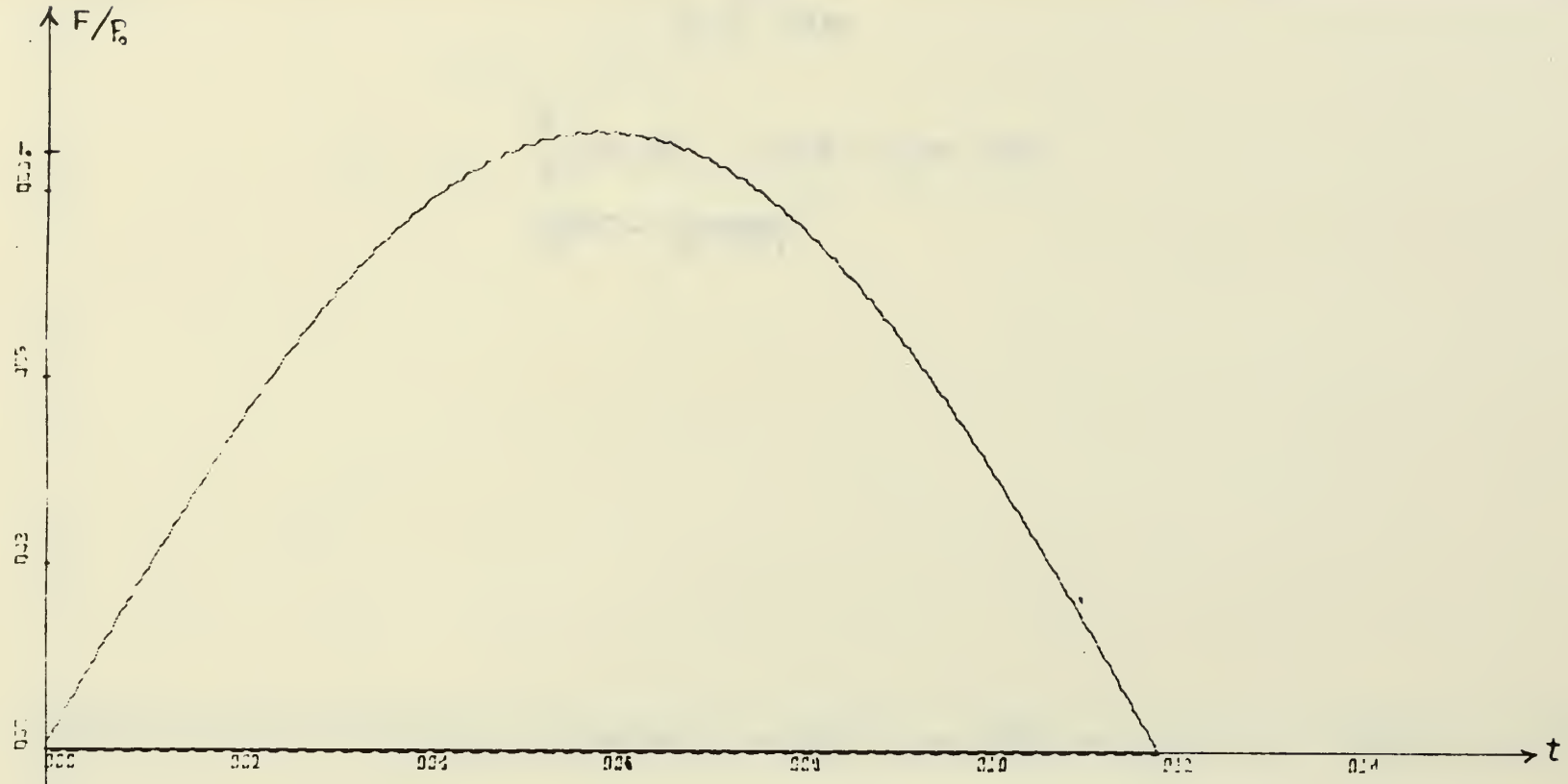

Free-Fixed

$\frac{x}{l} = .25 \quad \alpha = .012$ sec.

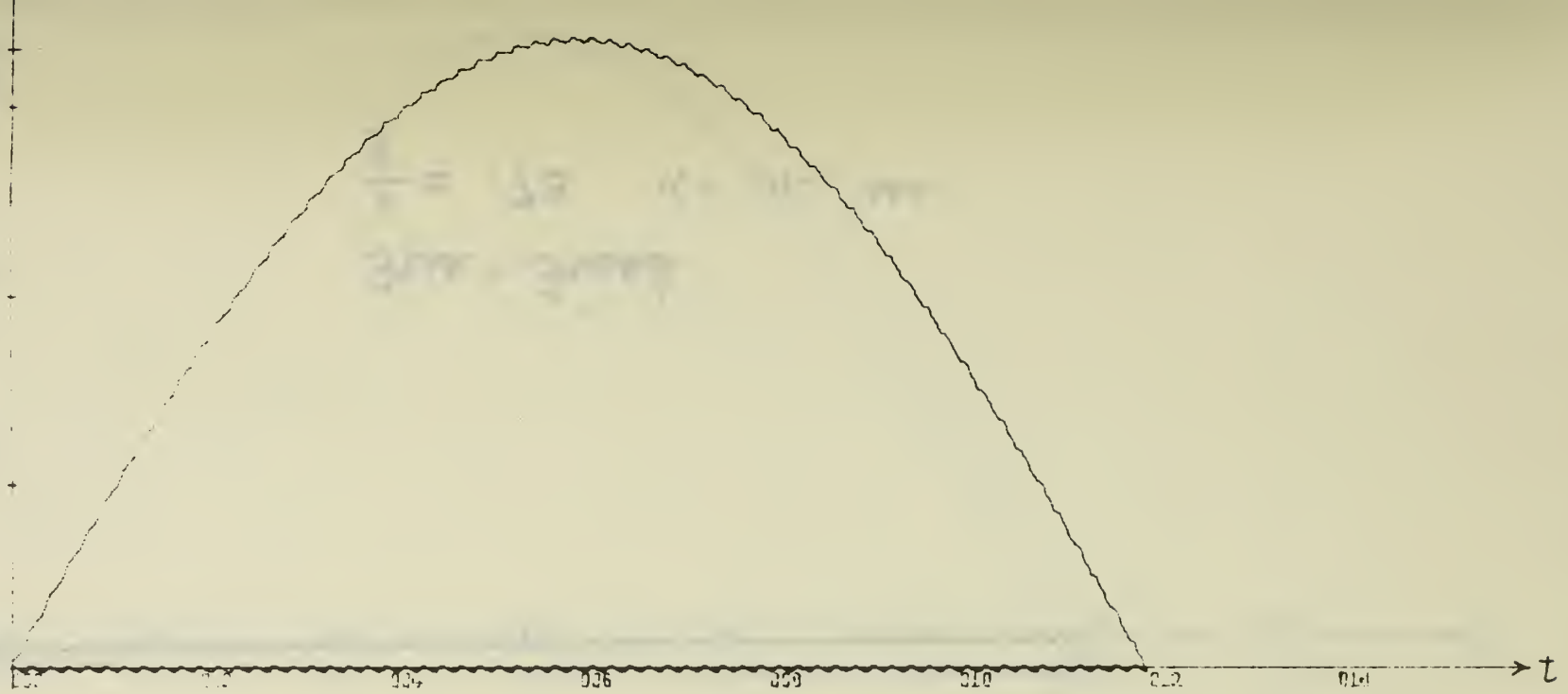

Free - Fixed

$\frac{x}{l} = 0.5 \quad \alpha = .012$ sec.

Fig. A8

Free - Fixed

$\frac{x}{\ell} = .75 \quad \alpha = .012$ sec.

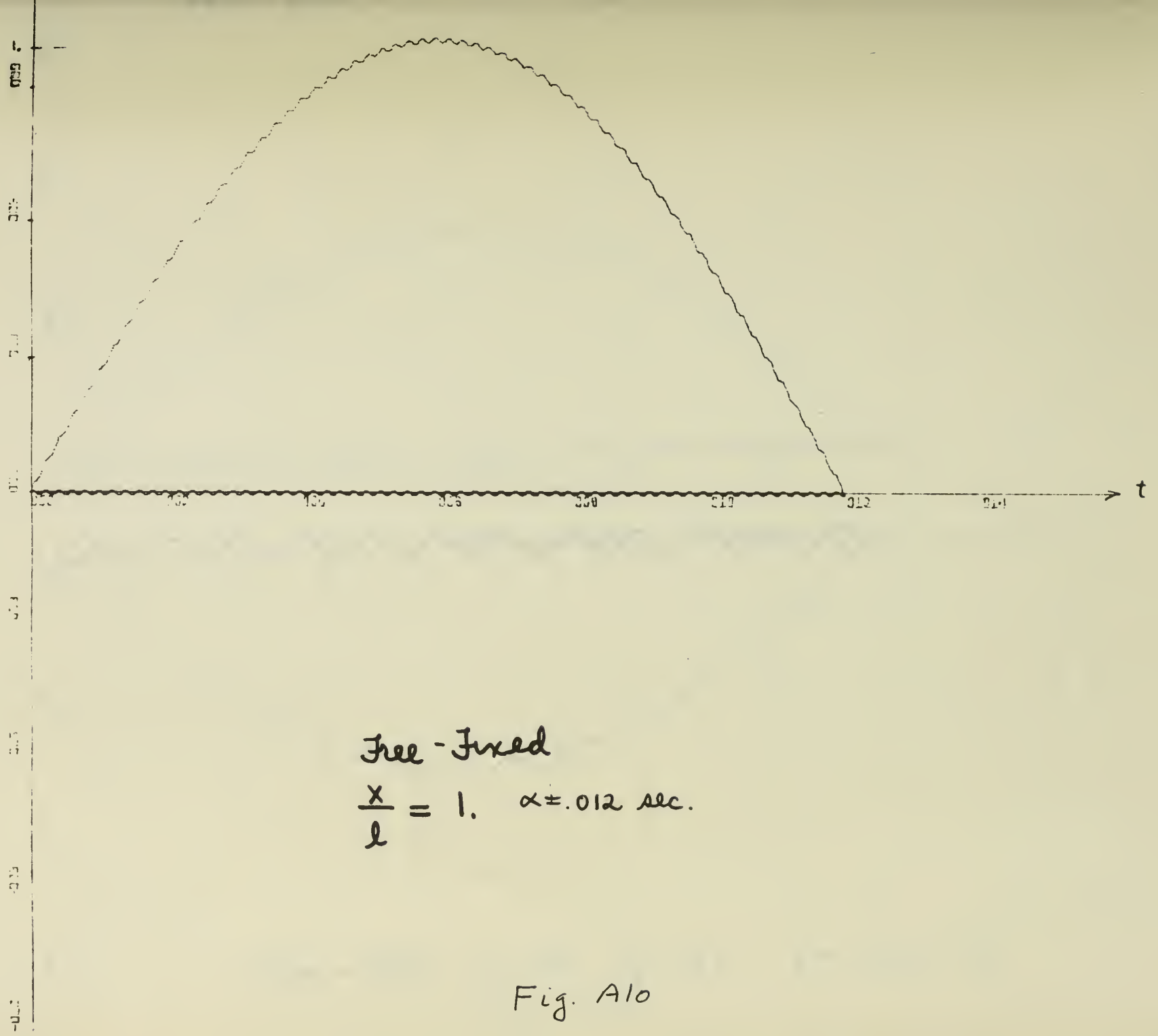

Free - Fixed

$\frac{x}{l} = 1.$ $\alpha = .012$ sec.

Fig. A10

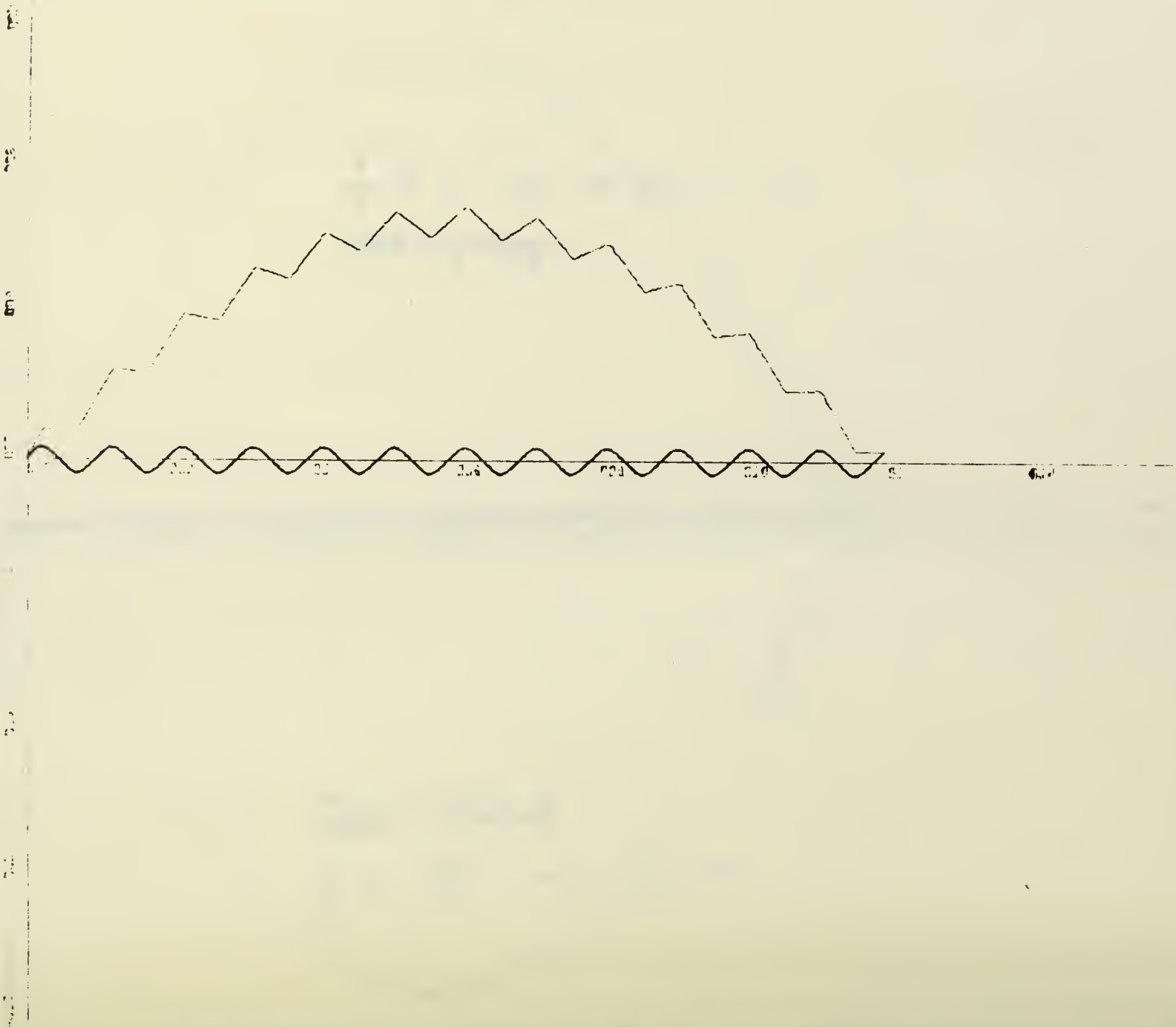

FREE-FREE $\alpha = .0012$ $\frac{X}{\ell} = .5$ Fig. A11

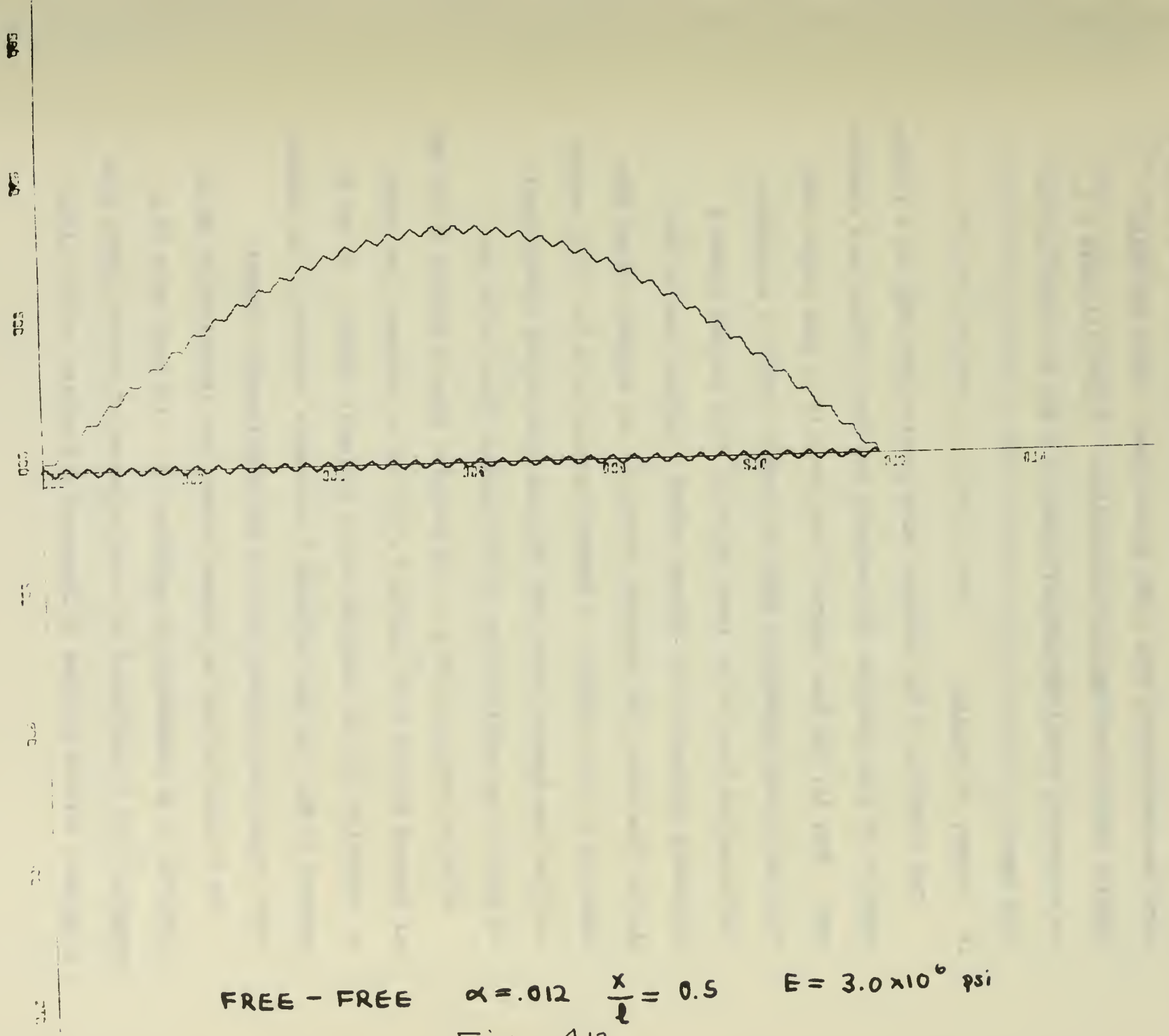

FREE - FREE $\alpha = .012$ $\frac{x}{\ell} = 0.5$ $E = 3.0 \times 10^6$ psi

Fig. A12

was plotted after each new term in the series was added. The solution with the contribution from U was plotted last. Hence the small wiggles indicate the dynamic contributions. Figure A13 shows F/P_o as a function of x/ℓ for several values of t for α = 0.012 sec. for both bars.

IV. Summary of Results

The solutions of the boundary value problem show that for a forcing function of time duration .012 seconds, the force appears as a standing wave. That is, the time length of the force is so much larger than the time of wave propagation that the dynamic effect is negligible. Decreasing the time of the force pulse to .0012 seconds showed a noticeable increase in the dynamic effect. However even at this shorter time pulse, the internal forces are but slightly larger than those for α = .012 seconds. A further decrease of α to .00012 seconds show that the dynamic forces are the same order as the static result and there is an amplification of the internal force in the bar.

With the time pulse at α = .012 seconds, Young's modulus of the bar was reduced from 30×10^6 psi to 3×10^6 psi to determine the effect of "softening" the bar material due to inelastic effects. It can be observed in Fig. A12 that although a noticeable increase in the dynamic effect occurs the internal force is not significantly altered.

The conclusion that the dynamic effects are insignificant can be supported by an examination of equation (52). For each value of n, equation (52) is equivalent to a single degree of freedom system with a harmonic forcing function of frequency π/α rad/sec or 260 rad/sec

for α = 0.012 sec. The natural frequency of the single degree of freedom system is $cn\pi/\ell$. For ℓ = 10 and c = 2.02 x 10^5 in/sec, the lowest natural frequency is 63,500 rad/sec. Hence, the ratio of the forcing frequency to the lowest natural frequency is 0.0041. The magnification factor for this frequency ratio is essentially one, i.e. the case response in a static sense.

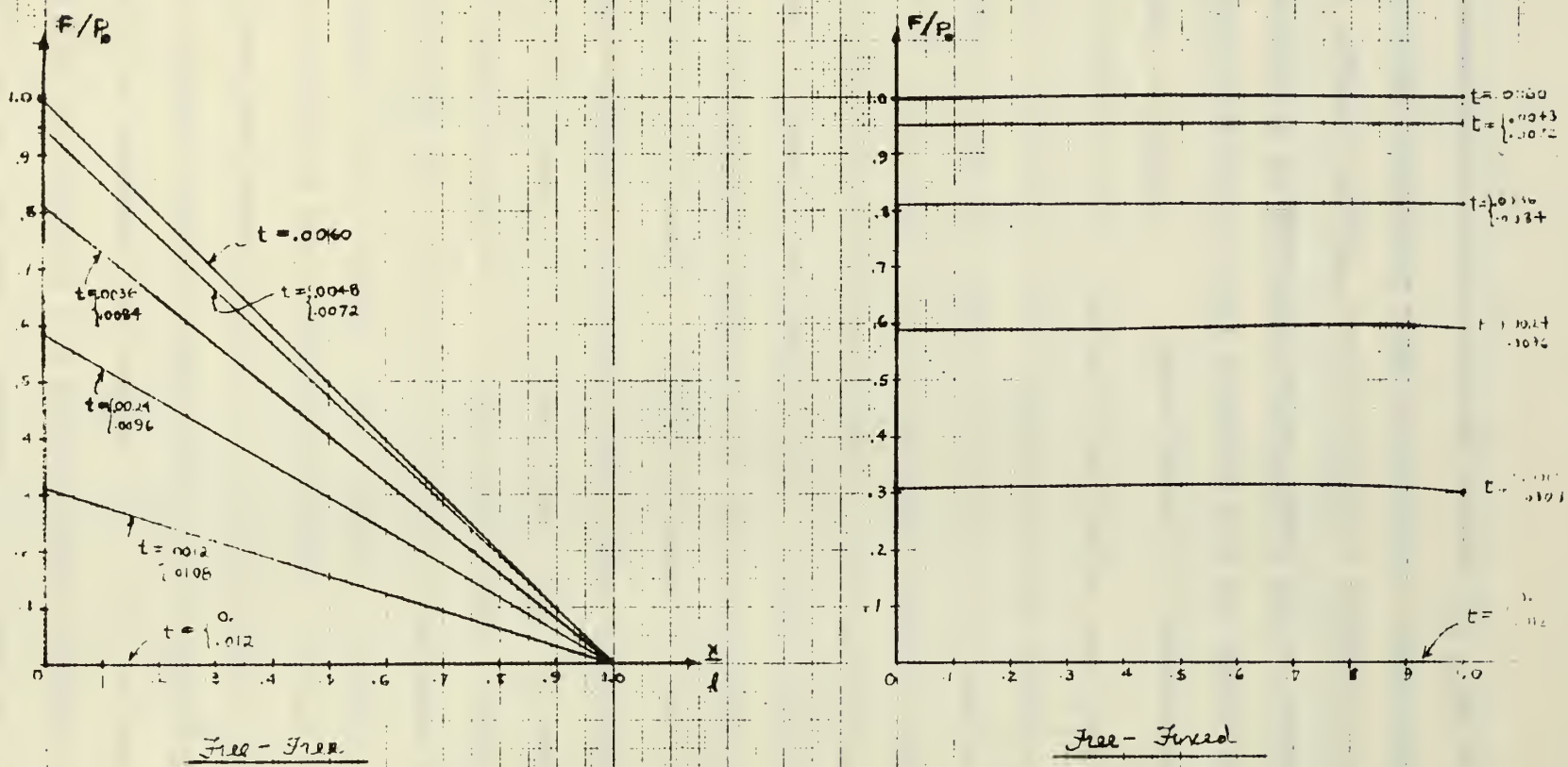

Free - Free

Free - Fixed

$\alpha = .012$ sec

A-28

Fig. A 13

APPENDIX B

Two-Dimensional Stress Analysis of the Motor Propellant

The results for the propellant-case interface stresses from the Rohm and Hass computer program AMG032A (Ref. 1) are given in Fig. B-1 for $E = 5 \times 10^5$ psi and a body force of 480 g, which is equivalent to an acceleration of 8000 g of the propellant grain whose density is 0.06 lb/in^3.* Also shown in Fig. B-1 is the location and the magnitude of the maximum principal tensile stress. In this analysis the motor case was assumed to be rigid. The nodes of the finite elements used to model the propellant are denoted in Fig. B-1 by I, J, where I defines the radial location and J the axial location as shown in Fig. B-1. The stresses predicted by the program are at the center of each element. Hence, the stresses shown in Fig. B-1 are actually located 0.125 in. from the propellant-case interface. A plot of the shear stress from the inner face of the propellant to the outer face is shown in Fig. B-2 for J = 14. Note that the outer face propellant shear stress is approximately 10% larger than the stress given in Fig. B-1 at J = 14.

The total vertical force provided by the longitudinal shear stress along the case and the axial compression stress on the bulkhead at the aft end is

---

*The computer program output consists of the coordinates and displacements of each nodal point and the stresses and strains for each continuum element.

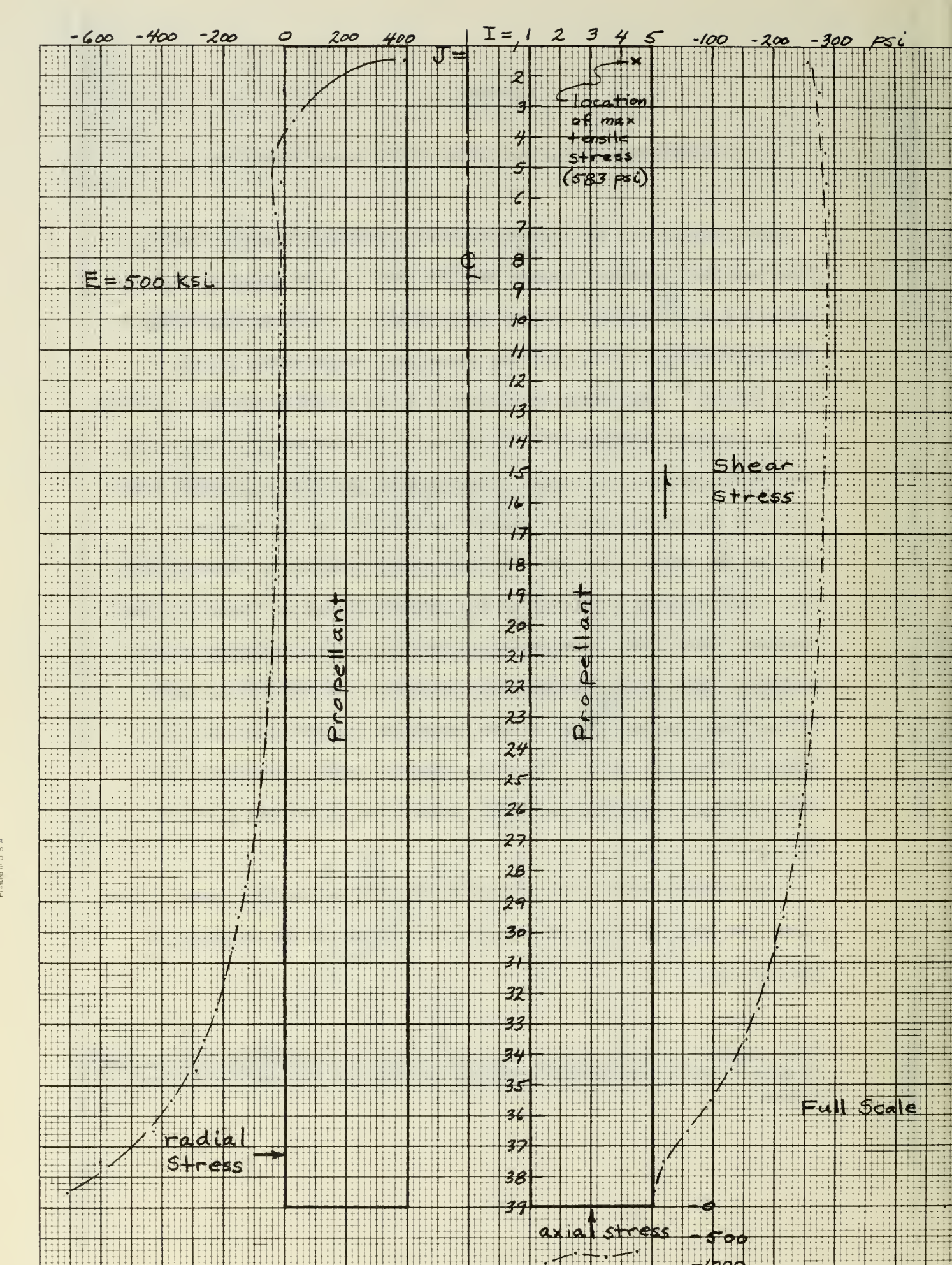

Fig. B-1 Propellant Stresses at Interface, Bonded

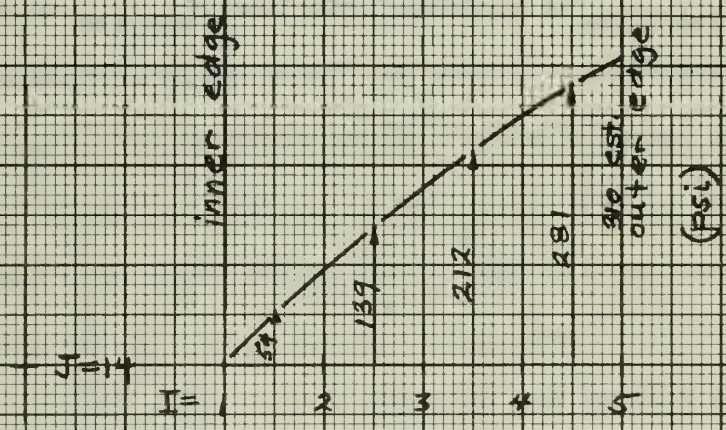

Fig. B-2 Shear Stress Distribution

$$P_{reaction} = (0.25 \text{ in.})(257 + 273 + \ldots 58 + 19 \text{ psi})(1.1)(\pi)(3 \text{ in.})$$
$$+ (0.25 \text{ in.})[(930 \text{ psi})(1.25 \text{ in.}) + (787 \text{ psi})(1.75 \text{ in.})$$
$$+ (832 \text{ psi})(2.25 \text{ in.}) + (731 \text{ psi})(2.75 \text{ in.})\text{psi}](\pi)$$
$$= 22.9 \text{ kips (shear)} + 5.0 \text{ kips (compression)} = 27.9 \text{ kips}$$

when the shear stresses shown in Fig. B-1 are increased by 10% to extrapolate to the interface stresses. The total force applied to the propellant is

$$P_{applied} = (0.06 \text{ lb/in.}^3)(1.5^2 - 0.5^2)(\text{in.}^2)(9.5 \text{ in.})(\pi)(8{,}000 \text{ g})$$
$$= 28.6 \text{ kips}$$

Thus, the stress analysis appears to provide total equilibrium. The fact that $P_{reaction}$ is slightly less than $P_{applied}$ is due to the fact that the compression stresses at the propellant-bulkhead interface are somewhat larger than the values shown in Fig. B-1, which are at the center of the bottom elements 0.125 in. above the bulkhead.

From these results $\frac{22.9}{27.9} = 82\%$ of the total propellant inertial load is carried by longitudinal shear stress on the motor case.

The same problem was analyzed with $E = 5 \times 10^4$ psi. The results were essentially identical.

The stresses for the unbonded propellant with $E = 5 \times 10^5$ psi are shown in Fig. B-3. The total vertical force is carried entirely by compression on the bulkhead at the aft end and is equal to

$$P_{reaction} = (0.25 \text{ in})[(4{,}418 \text{ psi})(1.25 \text{ in.}) + (4{,}490 \text{ psi})(1.75 \text{ in.})$$
$$+ (4{,}516 \text{ psi})(2.25 \text{ in.}) + (4{,}526 \text{ psi})(2.75 \text{ in.})](\pi)$$
$$= 28.2 \text{ kips}$$

The computer output for these three runs have been given to NWC personnel, Code 4573.

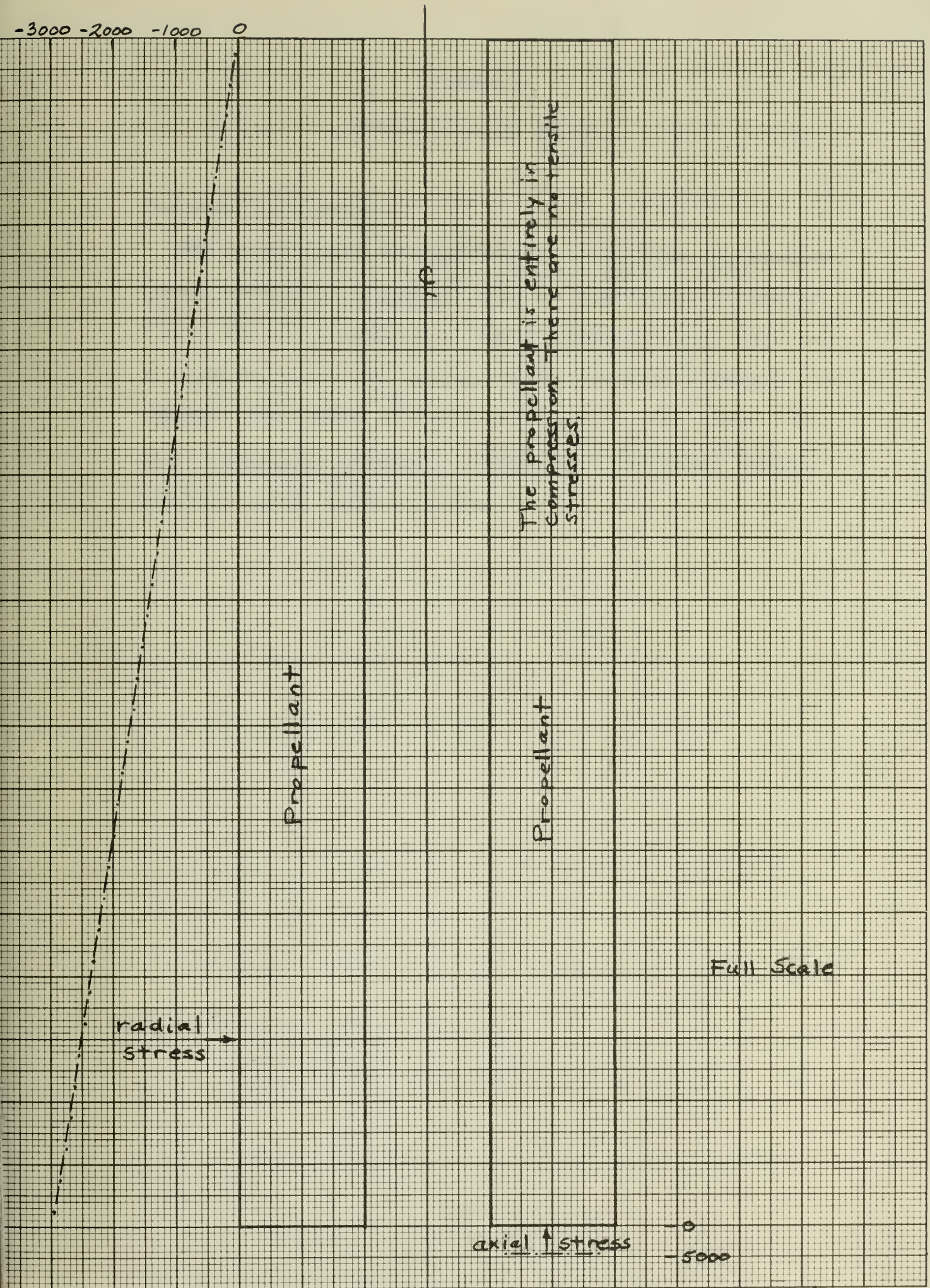

Fig. B-3 Propellant Stresses at Interface, Unbonded

APPENDIX C

Transient Lateral Motion

Statement of the Problem

The object of this investigation was to determine the transient lateral behavior of an axially loaded bar with initial deformation $w^i(x)$. The bar is idealized as simply supported at both ends, and is subjected to an axial compression $P(t) = P_o \sin \frac{\pi t}{\alpha}$ where $\alpha = .012$ seconds. The behavior of the bar was considered for various ratios of P_o, the maximum intensity of thrust, to P_e, the Euler buckling load for a simply supported column.

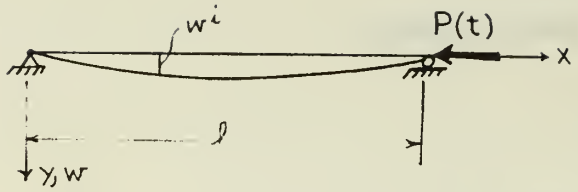

B.C.'s simply supported

w^i - initial imperfection, assume $w^i = \sum_{n=1}^{\infty} w_n^i \sin \frac{n\pi x}{\ell}$ (1)

w^d - bending deformation, assume $w^d = \sum_{n=1}^{\infty} f_n(t) \sin \frac{n\pi x}{\ell}$ (2)

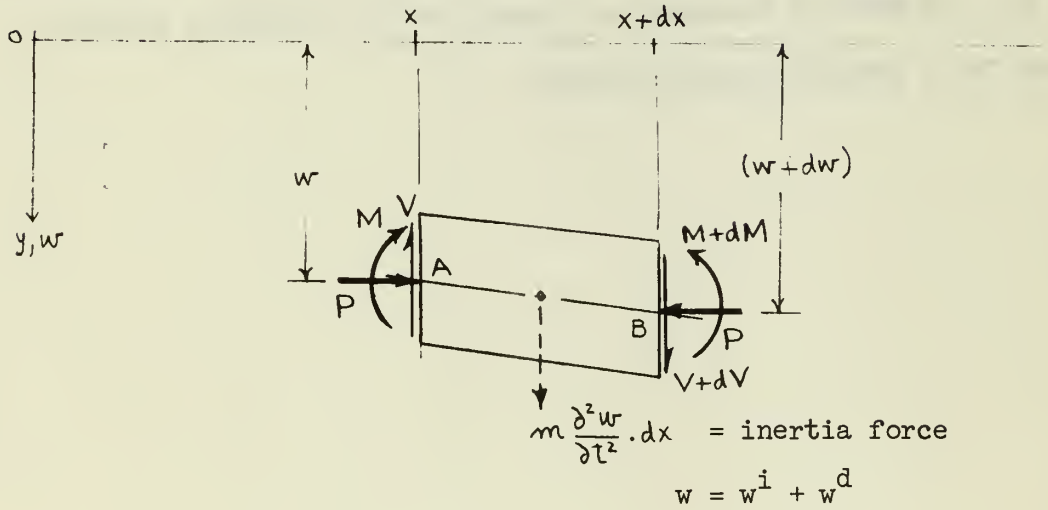

$w = w^i + w^d$

$$\sum M_A = 0: \quad M - (M + dM) + \frac{dx}{2}\left(m \frac{\partial^2 w}{\partial t^2}\right) + (V + dV)\, dx + P\, dw = 0$$

$$- \frac{dM}{dx} + V + \frac{P dw}{dx} = 0 \tag{3}$$

$$\sum V = 0: \quad V - (V + dV) - m \frac{\partial^2 w}{\partial t^2} dx = 0 \implies \frac{dV}{dx} = m \frac{\partial^2 w}{\partial t^2} \tag{4}$$

Recall the moment curvature relation,

$$M(x) = - EI\, w^{d}_{xx} \tag{5}$$

Using (3) and (5), equation (4) becomes

$$-EI \frac{\partial^4 w^d}{\partial x^4} - P \frac{\partial^2 w}{\partial x^2} = m \frac{\partial^2 w}{\partial t^2} \tag{6}$$

With (1), (2) and (7), equation (6) becomes

$$-\sum_{n=1}^{\infty} EI \left(\frac{n\pi}{\ell}\right)^4 f_n(t) \sin \frac{n\pi x}{\ell} + P(t) \sum_{n=1}^{\infty} \left(\frac{n\pi}{\ell}\right)^2 (w_n^i + f_n(t)) \sin \frac{n\pi x}{\ell}$$

$$= m \sum_{n=1}^{\infty} \ddot{f}_n(t) \sin \frac{n\pi x}{\ell} \tag{8}$$

which may be written

$$\sum_{n=1}^{\infty} \left[EI \left(\frac{n\pi}{\ell}\right)^4 f_n(t) - P(t) \left(\frac{n\pi}{\ell}\right)^2 (w_n^i + f_n(t)) + m \ddot{f}_n(t)\right] \sin \frac{n\pi x}{\ell} = 0 \tag{9}$$

$n = 1,2,\ldots$

Equation (9) is satisfied if each of the coefficients of $\sin \frac{n\pi x}{\ell}$ is zero, i.e.

$$EI \left(\frac{n\pi}{\ell}\right)^4 f_n(t) - P(t) \left(\frac{n\pi}{\ell}\right)^2 (w_n^i + f_n(t)) + m \ddot{f}_n(t) = 0 \tag{10}$$

with I.C.'s $$w(x,0) = w^i(x) \tag{11}$$

$$\frac{\partial w}{\partial t}(x,0) = v(x) \tag{12}$$

Using

$$P_e = \frac{n^2 \pi^2 EI}{\ell^2} \tag{13}$$

$$\omega_n = \frac{n^2 \pi^2}{\ell^2} \sqrt{\frac{EI}{m}} \tag{14}$$

equation (10) becomes

$$\ddot{f}_n(t) + \omega_n^2 \left(1 - \frac{P(t)}{P_e}\right) f_n(t) = \frac{P(t)}{P_e} \omega_n^2 w_n^i \tag{15}$$

$$n = 1,2,\ldots$$

with initial conditions,

$$f_n(0) = w_n^i \tag{16}$$

$$\dot{f}_n(0) = 0 \tag{17}$$

where

$$w_n^i = \int_0^\ell w^i(x) \sin \frac{n\pi x}{\ell} \, dx \tag{18}$$

For an impulse load in the form,

$$P(t) = P_o \sin \frac{\pi t}{.012} \tag{19}$$

and introducing the amplification factor

$$g_n(t) = \frac{f_n(t)}{w_n^i} \tag{20}$$

the previous system of equations become,

$$\ddot{g}_n(t) + \omega_n^2 \left[1 - \frac{P_o}{P_e} \sin \frac{\pi t}{.012}\right] g_n = \frac{P_o}{P_e} \sin \frac{\pi t}{.012} \omega_n^2$$

$$g_n(0) = 1 \tag{21}$$

$$\dot{g}_n(0) = 0$$

This equation is also valid for a cylindrical shell subjected to an axial load or an external pressure where ω_n is the natural frequency in the n^{th} mode and P_e is the buckling load in the n^{th} mode.

The previous system was solved numerically on the computer using a Runga-Kutta integration method to yield the results shown in Figs. C1-C9. Several values of P_o/P_e were considered for both ω_n = 6,000 rad/sec and 10,000 rad/sec.

Summary of Results

Amplification Factor $\|g(t)\|_{max}$		
P_o/P_e	ω = 6000 rad/sec	ω = 10,000 rad/sec
.75	3	4
.90	10	10
1.0	100	180
1.1	600	220,000
1.2	450,000	$\infty^{\ddagger}$
1.3	$\infty^{\ddagger}$	$\infty^{\ddagger}$

$^{\ddagger}\infty$ defined as greater than 1 x 10^{12} [maximum g(t) possible from computer integration algorithm.]

Estimation of the Natural Frequency*

$$\omega_n = \frac{K}{a}\sqrt{\frac{Gh}{m}\left(1 + \frac{\bar{K}^2}{K^2}\right)\frac{h^2}{a^2}}$$

m = mass/unit area

*From "Tables of Frequencies and Modes of Free Vibration of Infinitely Long Cylindrical Shells," by M. Barron and H. Bleich, J. Appl. Mech, Vol. 21, 1954, pp. 178-184.

where

$$a = 1.5 \text{ in.}$$

$$G = 11 \times 10^3 \text{ psi}$$

$$m = 7.43 \times 10^{-4} \frac{\#\text{-sec}}{\text{in}^4} \times .08 \text{ in.} = 5.94 \times 10^{-5} \frac{\#\text{-sec}^2}{\text{in}^3}$$

when the mass and elasticity of the propellant is neglected.

For $w = \sin \frac{\pi x}{\ell} \sin 2\theta$ $\quad (\frac{\ell}{a} = 6)$

$$K = 0.09178 \qquad \frac{\bar{K}^2}{K^2} = 2331$$

and hence

$$\omega = 9.6 \times 10^3 \text{ rad/sec}$$

Adding the mass of the propellant gives

$$m \approx 5.94 \times 10^{-5} + 1.38 \times 10^{-4} \times \pi \times 1.5^2/(3\pi) = 1.62 \times 10^{-4} \frac{\#\text{-sec}}{\text{in}^3}$$

Hence

$$\omega = 5.8 \times 10^3 \text{ rad/sec}$$

APPENDIX D

Computation of the Static Buckling Loads

Axial Compression Only (Ref. 2, page 528)

$$\frac{\sigma_{cr}}{\eta} = C_c \frac{Eh}{r}$$

where σ_{cr} is the design - allowable buckling stress, i.e., nine out of ten shells will not buckle at σ_{cr}. For elastic buckling $\eta = 1$. From Fig. 3.23-1, page 530 of Ref. 2.

$$C_c = 0.23$$

for $\frac{r}{h} = \frac{1.5}{0.08} = 18.8^*$ and

$$Z = \frac{L^2(1-\nu^2)^{1/2}}{rh} = \frac{(9.5)^2(1-.32^2)^{1/2}}{(1.5)(0.08)} = 715$$

Therefore

$$\frac{\sigma_{cr}}{\eta} = (0.23)\ (29 \times 10^3 \text{ ksi})\ (0.08 \text{ in.})/(1.5 \text{ in.})$$

$$= 356 \text{ ksi}$$

which is larger than σ_{cy}. Hence the buckling is inelastic, i.e. $\eta < 1$.

---

*This value of r/h is beyond the end of the curve, and hence the value selected for C_c is an estimated one. This indicates that perhaps this value is invalid for this small r/h ratio.

Figure 3.62-8, page 704 of Ref. 2, gives the critical inelastic buckling stress σ_{cr} as a function of σ_{cr}/η for elastic buckling for alloy steel 4130, heat treated to 180 ksi. From curve E_1,

$$\sigma_{cr} = 162 \text{ ksi}$$

This stress is based upon a 0.002 compressive yield stress of 164.5 ksi, which is considerably below the stresses of 179 ksi and 198 ksi given in MIL-HDBK-5A and for 4130 alloy steel heat treated to 180 ksi and 200 ksi respectively. Increasing the predicted critical inelastic buckling stress to account for the higher heat treatment leads to

$$\sigma_{cr} \approx (162 \text{ ksi}) \left(\frac{198}{179}\right) = 179 \text{ ksi}$$

when the MIL-HDBK stresses are used.

A static buckling test was conducted at NWC on an axially loaded 3 in. cylinder of 4130 alloy steel, heat treated with h = 0.065 in. For this cylinder,

$$\frac{\sigma_{cr}}{\eta} = 290 \text{ ksi}$$

and hence from Fig. 3.62-8 of Ref. 2 the inelastic buckling stress is

$$\sigma_{cr} = 159 \text{ ksi}$$

so that

$$\sigma_{cr} \approx (159 \text{ ksi}) \left(\frac{198}{179}\right) = 176 \text{ ksi}$$

From the experimental results, the axial force at buckling was 121.3 kips. Hence

$$(\sigma_{cr})_{exp} = \frac{121.3 \text{ kips}}{(\pi)(3 \text{ in.})(0.065 \text{ in.})} = 197.5 \text{ ksi}$$

which is considerably above the predicted value of 176 ksi and is essentially equal to σ_{cy}. This very high value is somewhat surprising. Nevertheless, in light of this the predicted inelastic buckling load of 179 ksi for the 0.08 in. case must be considered low (conservative).

External Radial Pressure Only (Ref. 2, page 540)

$$\frac{\sigma_{cr}}{\eta} = K_p \frac{\pi^2 E}{12(1-\nu^2)} \left(\frac{h}{L}\right)^2$$

From Fig. 3.23-7 of Ref. 2, lateral pressure only,

$$K_p = 24$$

for Z = 715. Therefore

$$\frac{\sigma_{cr}}{\eta} = (24) \frac{(\pi)^2 (29 \times 10^3 \text{ksi})(0.08 \text{ in.})^2}{(12)(1-.32^2)(9.5 \text{ in.})}$$

$$= 45 \text{ ksi}$$

which is below σ_{cy}. Hence, this buckling is elastic, and the critical lateral pressure is

$$q_{cr} = \frac{\sigma_{cr} h}{r} = (45 \text{ ksi}) \frac{(0.08 \text{ in.})}{(1.5 \text{ in.})} = 2.40 \text{ ksi}$$

DISTRIBUTION LIST

		No. Copies
1.	Defense Documentation Center Cameron Station Alexandria, Va 22314	20
2.	Library Code 0212 Naval Postgraduate School Monterey, Ca 93940	2
3.	Naval Weapons Center China Lake, Ca 93555	
	Attn: Howard Gerrish, Code 4545	1
	Ray Miller, Code 457	1
	Bob Dillinger/Dwight Weathersbee, Code 4573	1
4.	Naval Weapons Laboratory Dahlgren, Va	
	Attn: Ken Thorsted, Code GL	1
5.	Naval Ordnance Systems Command Navy Department Washington, D. C. 20350	
	Attn: J. Murrin, Code ORD 331	1
	Z. Levensteins, Code ORD 032	1
6.	Naval Air Systems Command Navy Department Washington, D. C. 20360	
	Attn: Code 320	1
7.	Asst. Prof. David Salinas Mechanical Engineering Department Naval Postgraduate School Monterey, Ca 93940	2
8.	Assoc. Prof. R. E. Ball Aeronautics Department Naval Postgraduate School Monterey, Ca 93940	2
9.	Chairman Department of Aeronautics Naval Postgraduate School Monterey, Ca 93940	1

10. Dean of Research Administration
Code 023
Naval Postgraduate School
Monterey, Ca 93940 — 1

DOCUMENT CONTROL DATA - R & D

(Security classification of title, body of abstract and indexing annotation must be entered when the overall report is classified)

1. ORIGINATING ACTIVITY *(Corporate author)*

Naval Postgraduate School
Monterey, California 93940

2a. REPORT SECURITY CLASSIFICATION

UNCLASSIFIED

2b. GROUP

3. REPORT TITLE

ANALYSIS OF A THREE INCH GUN LAUNCHED FINNED MOTOR CASE

4. DESCRIPTIVE NOTES *(Type of report and, inclusive dates)*

5. AUTHOR(S) *(First name, middle initial, last name)*

Robert E. Ball and David Salinas

6. REPORT DATE
28 January 1972

7a. TOTAL NO. OF PAGES
65

7b. NO. OF REFS
3

8a. CONTRACT OR GRANT NO.

b. PROJECT NO.

c.

d.

9a. ORIGINATOR'S REPORT NUMBER(S)
NPS-57BP72011A

9b. OTHER REPORT NO(S) *(Any other numbers that may be assigned this report)*

10. DISTRIBUTION STATEMENT

Approved for public release; distribution unlimited.

11. SUPPLEMENTARY NOTES

12. SPONSORING MILITARY ACTIVITY

13. ABSTRACT

An analysis of a 3-inch gun launched finned motor case is performed in an attempt to determine the cause of failure. Two specific features of the problem are identified as the probable reasons for the buckling failure of the motor case.

14 KEY WORDS	LINK A		LINK B		LINK C	
	ROLE	WT	ROLE	WT	ROLE	WT
buckling						
shells						
cylinders						
inelastic						
gun-launched projectiles						